



The Japanese Society of  
Microscopy



**MSC·SMC**

## Advanced Imaging and Analysis at Nanoscale

Japan-Canada Joint Seminar on Advanced Electron  
Microscopy and its application

-2<sup>nd</sup> Canada-Japan Microscopy Societies Symposium 2021-

November 15 - 17, 2021 (Canada)

11月, 16-18日, 2021年 (日本)

Virtual Event

[Click Here to Join Meeting](#)

**Zoom Meeting ID: 813 7163 6230**

**Passcode: 085804**

## Organizers

Canada (カナダ):

Marek Malac (NRC-NANO and Dept. of Physics, University of Alberta), Misa Hayashida (NRC-NANO), Alan Maigne (Stewart Blusson Quantum Matter Institute, University of British Columbia)

日本 (Japan):

森 茂生 Mori Shigeo (Osaka Prefecture University), 原田 研 Harada Ken (RIKEN)

## Sponsors

**HITACHI**  
Inspire the Next



**SOQUELEC**



Half part of this symposium managed in Japan was supported by JSPS-bilateral program.  
(JPJSBP220209905)

The goal of the workshop is to identify joint scientific interests and to promote scientific collaborations among MSC and JSM members. This year, the aim is to expand awareness of JSM and MSC members on the development of advanced electron and ion microscopy tools, methods and applications. New developments in instrumentation, improved understanding of fundamental limits of electron and ion microscopy and new tools and methods in data processing and their applications are welcome.



**Message from Microscopical Society of Canada president,  
Prof. Kathryn Grandfield**

Dear colleagues,

On behalf of the Microscopical Society of Canada (MSC), it is my honour to welcome you to the second annual Japan Microscopy Society (JSM) and MSC Symposium. This year's theme on Advanced Imaging and Analysis at the Nanoscale marks an exciting exchange between our societies sure to enhance our collaborations and pursuit of new research methods in microscopy. I congratulate the organizers on assembling such an exciting scientific panel and virtual meeting. I wish all attendees an inspiring and successful conference. We hope to meet in person next year!

Kathryn Grandfield  
President, Microscopical Society of Canada



**Message from Japanese Society of Microscopy president,  
Yuichi Ikuhara 先生**

Last year, the Japanese Society of Microscopy (JSM) planned JSM and the Microscopy Society of Canada (MSC) joint symposium on “Advanced Electron Microscopy and Its Application”. This symposium was initially organized by two countries collaboration program supported by JSPS (Japan Society for the Promotion of Science). But, unfortunately, we were forced to cancel this symposium due to the global spread of coronavirus infections (COVID-19). However, several voluntary members from JSM and MSC have continued to find a chance to organize JSM-MSC symposium to further enhance the international exchange and mutual collaboration between two countries as soon as possible. Finally, they have reached the conclusion to organize the virtual symposium on “Advanced Imaging and Analysis at Nanoscale” as the second Canada -Japan Microscopy Societies Symposium 2021. This symposium includes new developments in instrumentation, improved understanding of fundamental limits of electron and ion microscopy, new tools and methods in data processing and their applications, and also coincides with one of JSM policies “Internationalization”. I hope this symposium will be successfully held to further strengthen the relationships between the two countries.

Finally, I sincerely thank Prof. Shigeo Mori and Dr. Ken Harada from JSM and Prof. Marek Malac, the former president of MSC, Dr. Misa Hayashida and Dr. Alan Maigné from MSC for their big effort to organize this wonderful symposium.

**Yuichi Ikuhara**  
**President, Japanese Society of Microscopy**

## Message from symposium organizers

As the announcement implies, this is the *second* joint symposium of the Japanese Society of Microscopy (JSM) and the Microscopy Society of Canada (MSC). This year, the topic is “Advanced Imaging and Analysis at Nanoscale”. We are grateful to have received excellent scientific contributions from both the young generation as well as the pioneers of electron microscopy. We are particularly pleased to have a special guest speaker, Prof. Sumio Iijima, of the carbon nanotube fame.

Our long term goal is to help build scientist-to-scientist connections between JSM and MSC. A joint annual symposium is but a small step towards researcher visits that could bring further exciting science.

Covid-19 forced us to opt for a virtual rather than in-person meeting once again. (Although the case can be made that the virtual world weather is more pleasant than November in Edmonton.) Hopefully, the next JSM-MSC meeting will be held in person as early as 2022.

We are grateful for the sponsorship support of this year's symposium. It was kindly provided by Hitachi High Tech Canada and by Soquelec Ltd., who represent JEOL in Canada. Extensive thanks belongs to personnel who helped with practical aspects of the symposium. They are, Catherine Vachon and Michelle Hiltz at NRC-NANO, 眞田春佳 (Sanada Haruka) at Osaka Prefecture University and 眞田恵子 (Shimada Keiko) at RIKEN.

Please stay tuned for the 3<sup>rd</sup> annual joint symposium that will be held in 2022.

The JSM-MSC organizing committee working for you in both Canada and Japan,  
Marek Malac, Misa Hayashida, Alan Maigne, 森 茂生(Mori Shigeo), 原田 研 (Harada Ken)

## SCHEDULE

Join Zoom Meeting: <https://us02web.zoom.us/j/81371636230?pwd=RVRBNZ3M2p2bm1HdzVEVVPjN3E1dz09>

**Meeting ID: 813 7163 6230      Passcode: 085804**

Canada Edmonton UTC (-7hr)	Canada Eastern time UTC (-5 hr)	November 15, 2021 (Monday in Edmonton) 16, 火曜日 東京	November 16, 2021 (Tuesday in Edmonton) 17, 水曜日 東京	November 17, 2021 (Wednesday in Edmonton) 18, 木曜日 東京	東京 (Tokyo) UTC (+9 hr)
		Chair: Alan Maigné, Ken Harada	Chair: Shigeo Mori, Misa Hayashida	Chair: Alan Maigné, Shigeo Mori, Ken Harada	
3:50 – 4:00 pm	5:50 – 6:00 pm	Welcome & logistics <b>Ken Harada &amp; Marek Malac</b>	Welcome	Welcome	7:50 – 8:00 am
4:00 – 4:20 pm	6:00 – 6:20 pm	<b>Plenary Session</b>  <b>Ray Egerton</b> <b>What Determines the Spatial Resolution in Microscopy?</b>	<b>Arthur Blackburn</b> Application of 4D-STEM at 30 kV for structure analysis of block co-polymers and high-resolution multi-slice phase retrieval	<b>Plenary Session</b>  <b>Maureen Lagos</b>	8:00 – 8:20 am
4:00 – 4:20 pm	6:00 – 6:40 pm	<i>Zoom photo of participants (3 minutes)</i>	<b>Koji Harano</b> Visual Molecular Science at Interface of Self-Assembly and Electron Microscopy	<b>Phonon spectroscopy and Imaging at the Nanoscale</b>	8:20 – 8:40 am
4:40 – 5:00 pm	6:40 – 7:00 pm	<b>Plenary Session</b>  <b>Sumio Iijima</b>	<b>Plenary Session</b>  <b>Yuichi Ikuhara</b>	<b>Jun Yamasaki</b> TEM/STEM Intensity Modulation with Increasing Thickness Induced by Electron Multiple Scattering Phenomena in Materials	8:40 – 9:00 am
5:00 – 5:20 pm	7:00 – 7:20 pm	<b>Atomic resolution STEM-EDS imaging of cations ordering of Ti-Nb and Nb-W ternary oxides for LIBs anodes</b>	<b>Atomic-Scale Dynamic Observations of Interface, Surface and Grain Boundary Phenomena</b>	<b>Marek Malac</b> NanoMi: a Public-License Platform for Electron Microscopy Development and Education	9:00 – 9:20 am
5:20 – 5:40 pm	7:20 – 7:40 pm	<b>Raynald Gauvin</b> EDS and EELS of Lithium Materials from 0.5 to 30 keV	<b>Roghayeh Nikbakht</b> Contribution of microstructure in oblique impact morphology of high entropy CrMnCoFeNi particles	<b>Junji Yamanaka</b> STEM-Moiré Applications to Crystalline Specimens without using High-End Microscopes	9:20 – 9:40 am
5:40 – 6:00 pm	7:40 – 8:00 pm	<b>Nadi Braidy</b> Progress on Multivariate Statistics to Improve Spectrum Image Interpretation	<b>Yoshifumi Oshima</b> Atomic bond stiffness in Pt atomic chains measured by TEM coupled with a quartz LER	<b>Alan Maigné</b> Development of Electron Microscopy toward Analysis of Optical and Quantum Effects in Nanomaterials.	9:40 – 10:00 am
6:00 – 6:20 pm	8:00 – 8:20 pm	<b>Kohei Aso</b> Data-Driven Electron Microscopy Reveals Shape-Dependent Subpercent Strains in Gold Nanorods	<b>Xuan Quy Tran</b> Thermal Evolution of Alloying State in Ternary IrPdRu Nanoparticles	<b>Hiroshi Okamoto</b> TEM at Millikelvin Temperatures: What Would It Be Useful for?	10:00 – 10:20 am
6:20 – 6:40 pm	8:20 – 8:40 pm	<b>Anitha Jose</b> Mapping electrostatic potential gradient in GaN NW p-n junctions using electron holography.	<b>Alyssa Williams</b> Utilization of Correlative Light and Electron Microscopy for Analyzing the Structural Organization of Bacterial Microcrystalline Cellulose.	<b>Misa Hayashida</b> Higher-order structure of barley chromosomes observed by Electron Tomography	10:20 – 10:40 am
6:40 – 7:00 pm	8:40 – 9:00 pm	<b>Takayuki Nakamuro</b> Capturing the moment of nucleation and tracing the crystal growth by SMART-EM	<b>Mohammadparsa Khakpour</b> Manual versus automatic analysis of microglial spatial characteristics: a comparison in the hippocampus of healthy adult mice	<b>Tomokazu Yamamoto</b> In-situ STEM observation of Ni catalyst during dry methane reforming	10:40 – 11:00 am
7:00 – 7:20 pm	9:00 – 9:20 pm	<b>Rodney Herring</b> Phase Imaging Electron Intensities on the Diffraction Plane	<b>Ben Cardoen</b> Belief theory enables detection of Caveolae in superresolution microscopy.	<b>Hesham El-Sherif</b> STEM and EELS of Spontaneous Incommensurate van der Waals Heteroepitaxy	11:00 – 11:20 am
7:20 – 7:25 pm	9:20 – 9:25 pm			Closing remarks <b>Ken Harada, Misa Hayashida</b>	11:20 – 11:25 am

Zoom/Conference hosts [Catherine.Vachon@nrc-cnrc.gc.ca](mailto:Catherine.Vachon@nrc-cnrc.gc.ca) or [Michelle.Hiltz@nrc-cnrc.gc.ca](mailto:Michelle.Hiltz@nrc-cnrc.gc.ca)

## BOOK OF ABSTRACTS-TABLE OF CONTENTS

### Plenary Sessions

<b>Day 1</b> Ray Egerton What Determines the Spatial Resolution in Microscopy?	Page 12
<b>Day 1</b> Sumio Iijima Atomic resolution STEM-EDS imaging of cations ordering of Ti-Nb and Nb-W ternary oxides for LIBs anodes.	Page 13
<b>Day 2</b> Yuichi Ikuhara Atomic-Scale Dynamic Observations of Interface, Surface and Grain Boundary Phenomena.	Page 14
<b>Day 3</b> Maureen Lagos Phonon spectroscopy and Imaging at the Nanoscale.	Page 15

## Day 1 Abstracts

Raynald Gauvin EDS and EELS of Lithium Materials from 0.5 to 30 keV.	Page 16
Nadi Braidy Progress on Multivariate Statistics to Improve Spectrum Image Interpretation.	Page 17
Kohei Aso Data-Driven Electron Microscopy Reveals Shape-Dependent Subpercent Strains in Gold Nanorods.	Page 18
Anitha Jose Mapping electrostatic potential gradient in GaN NW p-n junctions using electron holography.	Page 19
Takayuki Nakamuro Capturing the moment of nucleation and tracing the crystal growth by SMART-EM.	Page 20
Rodney Herring Phase Imaging Electron Intensities on the Diffraction Plane.	Page 21

## Day 2 Abstracts

Arthur Blackburn Application of 4D-STEM at 30 kV for structure analysis of block co-polymers and high-resolution multi-slice phase retrieval.	Page 22
Koji Harano Visual Molecular Science at Interface of Self-Assembly and Electron Microscopy.	Page 23
Roghayeh Nikbakht Contribution of microstructure in oblique impact morphology of high entropy CrMnCoFeNi particles.	Page 24
Yoshifumi Oshima Atomic bond stiffness in Pt atomic chains measured by TEM coupled with a quartz LER.	Page 25
Xuan Quy Tran Thermal Evolution of Alloying State in Ternary IrPdRu Nanoparticles.	Page 26
Alyssa Williams Utilization of Correlative Light and Electron Microscopy for Analyzing the Structural Organization of Bacterial Microcrystalline Cellulose.	Page 27
Mohammadparsa Khakpour Manual versus automatic analysis of microglial spatial characteristics: a comparison in the hippocampus of healthy adult mice.	Page 28
Ben Cardoen Belief theory enables detection of Caveolae in superresolution microscopy.	Page 29

### Day 3 Abstracts

Jun Yamasaki TEM/STEM Intensity Modulation with Increasing Thickness Induced by Electron Multiple Scattering Phenomena in Materials.	Page 30
Marek Malac NanoMi: a Public-License Platform for Electron Microscopy Development and Education.	Page 31
Junji Yamanaka STEM-Moiré Applications to Crystalline Specimens without using High-End Microscopes.	Page 32
Alan Maigné Development of Electron Microscopy toward Analysis of Optical and Quantum Effects in Nanomaterials.	Page 33
Hiroshi Okamoto TEM at Millikelvin Temperatures: What Would It Be Useful for?	Page 34
Misa Hayashida Higher-order structure of barley chromosomes observed by Electron Tomography.	Page 35
Tomokazu Yamamoto In-situ STEM observation of Ni catalyst during dry methane reforming.	Page 36
Hesham El-Sherif STEM and EELS of Spontaneous Incommensurate van der Waals Heteroepitaxy.	Page 37

## What Determines the Spatial Resolution in Microscopy?

Ray Egerton \*

<sup>1</sup> Physics Department, University of Alberta, Edmonton, AB T1W 2E2, Canada.

\*regerton@ualberta.ca

As usual, the answer depends on how you phrase the question, but we can identify the following factors as being of particular importance for electron microscopes.

**Lens optics**, including the presence of apertures and/or aberration correctors.

**Microscope environment**, including vibrations, pressure and temperature changes.

**Power-supply stability**, readout speed.

**Beam spreading**, important in STEM and EDX imaging.

**Coulomb delocalization**, sometimes important for EELS studies.

**Electron statistics and radiation damage**, critical for some specimens.

These questions will be addressed in turn but the main purpose of the talk will be to advocate the use of a **point-spread function (PSF)** for specifying resolution [1], and **dose-limited resolution (DLR)** in the case of beam-sensitive specimens [2]. Some examples are shown below.

References:

[1] R F Egerton, Ultramicroscopy, Vol.145, (2014), pages 85-93.

[2] R F Egerton, Micron, Vol.119, (2019), pages 72-87.

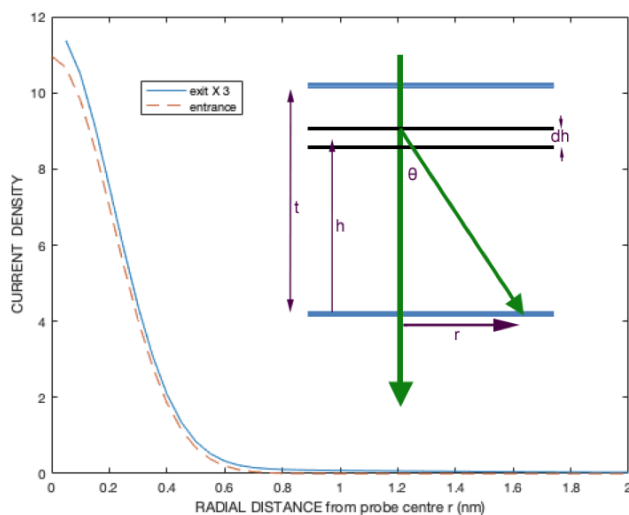


Fig. 1 PSF for beam spreading (solid blue curve) calculated for 100keV electrons at the exit surface of a 100nm sample of amorphous silicon. The tails of this function arise from elastic scattering and contribute 60% of the integrated intensity.

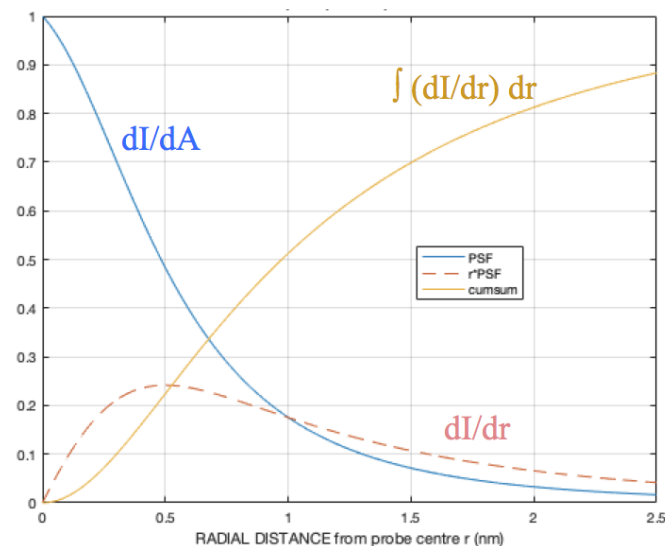


Fig. 2. PSF for Coulomb delocalization of 100keV electrons (blue curve), calculated for an energy loss of 25 eV and  $FWHM = 25/k_0\theta_E$ . The red dashed curve represents electron intensity per unit radius and the yellow curve is its cumulative sum.

# Atomic resolution STEM-EDS imaging of cations ordering of Ti-Nb and Nb-W ternary oxides for LIBs anodes

Sumio Iijima<sup>1\*</sup>, Zheng Liu<sup>2</sup>, Ichiro Ohnishi<sup>3</sup>, Wenhui Yang<sup>4</sup> & Syo Matsumura<sup>4</sup>

<sup>1</sup>Meijo University, Graduate School of Science and Technology, Nagoya 468-8502, Japan

<sup>2</sup>Innovative Functional Materials Research Institute, National Institute of Advanced Industrial Science and Technology (AIST), Nagoya 463-8560, Japan

<sup>3</sup>JEOL Ltd., 3-1-2 Musashino, Akishima, Tokyo 196-8558, Japan

<sup>4</sup>Kyushu University, Department of Applied Quantum Physics and Nuclear Engineering, Fukuoka 819-0394, Japan

\*ijimas@meijo-u.ac.jp

Atomic resolution STEM-EDS imaging method is used to solve order-disorder problems in complex metal oxide crystals, supplementing conventional X-ray or neutron diffraction. The materials were ternary metal oxides  $\text{Ti}_2\text{Nb}_{10}\text{O}_{29}$  and  $4\text{Nb}_2\text{O}_5 \cdot 9\text{WO}_3$  ( $2\text{Nb}_2\text{O}_5 \cdot 7\text{WO}_3$ ), which have recently attracted attention as energy storage materials in lithium-ion batteries. The most of LIBs researchers assumed these ternary oxides to be solid-solution and did not pay attention to cation chemical ordering. Our study reveals the presence of obvious chemical ordering of metal ions in these materials and the relative occupancies of cations at each metal atom site were determined directly from the EDS images taken by JEM-ARM300F operated at 300kV. Towards quantification of the atomic EDS images we investigated an effect of electron channeling at individual atomic columns.

- 1) Sumio Iijima, Ichiro Ohnishi, Wenhui Yang and Syo Matsumura, *Comm. Mater.*, **2**, 1-9 (2021).
- 2) Sumio Iijima, Ichiro Ohnishi and Zheng Liu, *Scientific Reports*, **11**, 1-11 (2021).

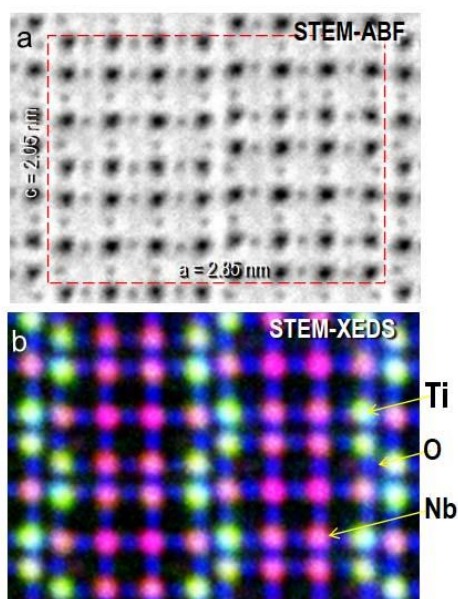


Figure 1. (a) A STEM-ABF image of a  $\text{Ti}_2\text{Nb}_{10}\text{O}_{29}$  crystal in the [010] orientation, showing the metal atomic columns and oxygen (faint dots). (b) A STEM-EDS overlay crystal image recorded using the Ti  $K\alpha$  emission (green), Nb  $L\alpha$  (red) and O  $K\alpha$  (blue), showing a segregation of the metal atomic columns in an ordered fashion.

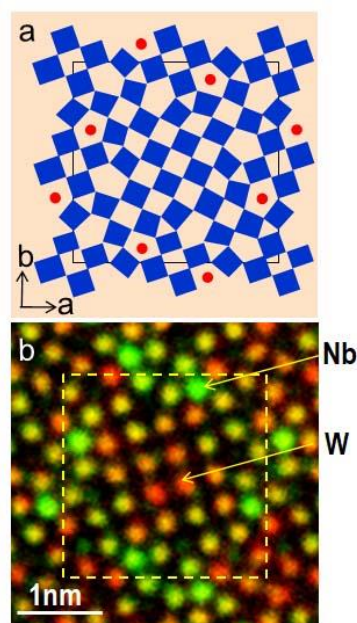


Fig. 2. Atomic resolution STEM-EDS image of a crystal of  $2\text{Nb}_2\text{O}_5 \cdot 7\text{WO}_3$ . (a) A schematic model of the crystal. (b) A STEM-EDS overlay image recorded using the Nb  $L\alpha$  X-ray (green) and W  $M\alpha$  X-ray (red) lines, which corresponds to the model depicted in panel (a).

# Atomic-Scale Dynamic Observations of Interface, Surface and Grain Boundary Phenomena

Yuichi Ikuhara<sup>1, 2, 3\*</sup>

<sup>1</sup>Institute of Engineering Innovation, University of Tokyo, Tokyo 113-8656, Japan

<sup>2</sup>Nanostructures Research Laboratory, Japan Fine Ceramics Center, Nagoya, 456-8587, Japan

<sup>3</sup>WPI Research Center, AIMR, Tohoku University, Sendai, 980-8577, Japan

\*[ikuhara@sigma.t.u-tokyo.ac.jp](mailto:ikuhara@sigma.t.u-tokyo.ac.jp)

Materials properties depend on the dynamic behavior under various conditions such as temperature, stress, atmosphere. For example, mechanical properties of polycrystals are influenced by the interaction of grain boundary, dislocation and crack. On the other hand, functional properties are often influenced by ion diffusion at service temperatures. So far, many atomic scale observations have been performed for understanding fracture, deformation, diffusion and so on, but these experiments were mostly carried out statically, and the dynamic behavior is still not well understood yet. In addition, these dynamic behaviors often occur at interface and surface. In this study, the in-situ nanoindentation experiments were conducted for SrTiO<sub>3</sub> and Al<sub>2</sub>O<sub>3</sub> bicrystals inside TEM to understand their deformation process at the interfaces. For observing ion diffusion from the surface, single crystal of lithium ion battery (LIB) were used for the ex-situ experiment as a model system.

For observing dislocation-interface interaction, various types of GBs including CSL (Coincidence Site Lattice) GBs and low angle tilt and twist GBs for SrTiO<sub>3</sub> and Al<sub>2</sub>O<sub>3</sub> were systematically prepared. Various interface phenomena such as dislocation pile-up at GBs, jog formation, jog-drag motion, deformation twinning were dynamically observed by these experiments. The dislocation-GB interaction and its dependence on the GB characters, the propagation mechanism of deformation twinning will be discussed in detail. In addition, the crack propagation behavior of Zr-doped Al<sub>2</sub>O<sub>3</sub> GB was directly observed, and the as-fractured wall surfaces were characterized by Cs corrected STEM. It was found that the crack propagated in zigzag manner within the segregated Zr atom layers. The relationship of the atomic-scale crack propagation path and the grain boundary structure will be discussed in detail.

The properties of lithium ion battery (LIB) cathodes strongly depend on the dynamic diffusion of lithium ions during charge/discharge process. Then, direct visualization of lithium site is required to understand the mechanism of the diffusion of lithium ions. In this study, Cs corrected STEM were applied to directly observe the {010} surface, which corresponded to perpendicular to the 1-D diffusion orientation, of the olivine Li<sub>x</sub>FePO<sub>4</sub>. Commercially available LiFePO<sub>4</sub> single crystals were used for all experiments. The crystals were cut perpendicular to their <010> axis and polished, and the structures of {010} surfaces before and after chemical delithiation were characterized by STEM. It was found that orientation of boundary layers at the FePO<sub>4</sub>/LiFePO<sub>4</sub> interface gradually changed from lower index planes to higher index planes. The dynamic diffusion mechanism of the lithiation/delithiation from and to the surface will be discussed based on the observation results.

## References:

- [1] S. Kondo, T. Mitsuma, N. Shibata, Y. Ikuhara, *Sci. Adv.*, 2[11], e1501926 (2016).
- [2] S. Kondo, A. Ishihara, E. Tochigi, N. Shibata, and Y. Ikuhara, *Nature Commun.*, 10, 2112 (2019).
- [3] J. Wei, B. Feng, R. Ishikawa, T. Yokoi, K. Matsunaga, N. Shibata and Y. Ikuhara, *Nat. Mater.*, doi: 10.1038 / s41563-020-00879-z (2021).
- [4] S. Kobayashi, C.A. J. Fisher, T. Kato, Y. Ukyo, T. Hirayama and Y. Ikuhara, *Nano Lett.*, 16, 5409 (2016)
- [5] S. Kobayashi, A. Kuwabara, C. A. J. Fisher, Y. Ukyo and Y. Ikuhara, *Nat. Commun.*, 9, 2863 (2018)

## Phonon Spectroscopy and Imaging at the Nanoscale

Ka Y. Lee<sup>1</sup>, Zihan Lyu<sup>1</sup>, Elliot K. Beutler<sup>2</sup>, Ulrich Hohenester<sup>3</sup>, Philip E. Batson<sup>4</sup>, David J. Masiello<sup>2</sup>, Maureen J. Lagos<sup>1,5</sup>

<sup>1</sup> Department of Materials Science and Engineering, McMaster University, Hamilton, Canada.

<sup>2</sup> Department of Chemistry, University of Washington, Seattle, USA.

<sup>3</sup> Department of Physics, University of Graz, Graz, Austria.

<sup>4</sup> Department of Physics, Rutgers University, New Jersey, USA.

<sup>5</sup> Canadian Centre for Electron Microscopy, McMaster University, Hamilton, Canada.

\* mjlagos@mcmaster.ca

The development of monochromators implemented in STEMs has opened the doors for phonon/vibrational spectroscopy studies in nanomaterials using atom-wide monochromatic electron probes [1]. Instrumental developments are still in progress and energy resolutions of 3.7 meV at 60 kV were recently obtained [2]. As it is usual the case, vibrational EELS experiments are complex and data interpretation presents enormous challenges. But despite these barriers the EELS community has made significant progress in obtaining a much deeper understanding of the inelastic electron scattering by phonons in nanoscale systems. In this presentation, we will describe this progress by highlighting the following results: (i) imaging surface and bulk phonon modes in a single nanoparticle [3], (ii) plasmon-phonon coupling in infrared antennas [4], (iii) role of the substrate in the phonon response of nanoparticles [5], and (iv) the development of a thermometry methodology to measure local temperature in single nanostructures using energy-loss and energy-gain scattering [6]. Our results provide progress in understanding the excitation of surface and bulk phonons sustained in nanoscale volumes of matter using swift electrons.

### References:

- [1] T. Miyata, *et al*, *Microscopy* 63, (2014), 377. / O. Krivanek, *et al*, *Nature* 514, (2014), 209.
- [2] Private communication with Ondrej Krivanek and Tracy Lovejoy.
- [3] M. J. Lagos, *et al*, *Nature* 543, (2017), 529. / M. J. Lagos, *et al*, *Microscopy* 67, (2018), i3.
- [4] M. J. Lagos, *et al*, *ACS Photonics* 8, (2021), 1293.
- [5] E. K. Beutler, *et al*, *Physical Review B* 103, (2021), 165418.
- [6] M. J. Lagos and P. E. Batson, *NanoLetters* 18, (2018), 4556.
- [7] We acknowledge financial support of Canada NSERC.

## EDS and EELS of Lithium Materials from 0.5 to 30 keV

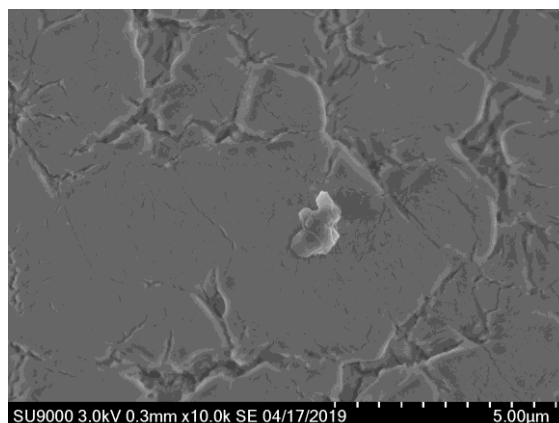
Raynald Gauvin<sup>1\*</sup>, Nicolas Brodusch<sup>1</sup> and Frédéric Voisard<sup>1</sup>

<sup>1</sup>McGill University, 3610 University, Montreal, Canada, H3A 0C5

This paper will present state of the art results acquired with the SU-9000 dedicated 30 keV (and less) STEM that has EELS capabilities. It has a resolution of 0,22 nm in bright field STEM without aberration correctors. It is equipped with an Extreme SDD EDS detector that allows Lithium detection. With EELS and EDS, results for Li detection will be presented and the challenges, in regards of quantification and beam damage, will be covered. Examples of EELS analysis at 30 keV for nanomaterials will be presented, including surface plasmon. The SU-9000EA allows to perform electron diffraction and CBED patterns acquired at the nanoscale will be presented.

As an example, figure 1 shows a LiCl specimen after an EDS spectrum was acquired. To detect the Li K line after 200 second acquisition time, the specimen had to be damaged by the beam. Understand the beam damage is critical for successful application of EDS for Li based materials.

Figure 1. LiCl specimen after the acquisition of a EDS Spectrum. 200 S live time.



## Progress on Multivariate Statistics to Improve Spectrum Image Interpretation

Nadi Braidy<sup>1,2\*</sup>, Ryan Gosselin<sup>1</sup>

<sup>1</sup> Chemical and Biotechnological Engineering, Université de Sherbrooke. 2500 Boul. de l'Université, Sherbrooke, Québec, J1K 2R1, Canada

<sup>2</sup> Institut Interdisciplinaire d'Innovation Technologique (3IT), Université de Sherbrooke. 3000 Boul. de l'Université, Sherbrooke, Québec, J1K 0A5, Canada.

\*nadi.braidy@usherbrooke.ca

TEM spectrum images are typically processed using background removal and peak-integration techniques. Latent variable models such as principal component analysis (PCA) and multivariate curve resolution alternating least-squares (MCR-ALS) are becoming interesting alternatives capable of resolving complex mixtures into pure component contributions. Recently [1,2], we proposed a new method for the analysis of low-count spectrum images [1] in which the multilinear regression step of the MCR-ALS is replaced by the Log-Likelihood Maximization (MCR-LLM) under spectral constraints based on Poisson noise characteristics.

We demonstrate the advantages of using the MCR-LLM method for the analysis of several datasets, including an EELS spectrum-image of ferrite nanoparticles exhibiting surface segregation (Fig 1, [3]), a simultaneously recorded EELS-EDX linescan from a transistor stack, and an EDX map from a III-V nanowire. Once the components are isolated, it becomes straightforward to conduct elemental and quantitative analyses. In addition to enabling the extraction of meaningful spectral components (unlike PCA), the MCR-LLM method makes it possible to carry out analyses of low signal-to-noise ratio dataset and co-registered datasets. For each instance, we will detail the analytical strategy and discuss the added value of such an approach and possible pitfalls.

### References:

[1] Lavoie, F. B., Braidy N. & Gosselin, R. Including noise characteristics in MCR to improve mapping and component extraction from spectral images. *Chemometrics and Intelligent Laboratory Systems* 153 (2016), 40

[2] Braidy, N. & Gosselin, R. Unmixing noisy co-registered spectrum images of multicomponent nanostructures. *Scientific Reports* 9, (2019), 1

[3] Li, A. Y., Dumaresq, N., Segalla, A., Braidy, N. & Moores, A. Plasma-Made (Ni<sub>0.5</sub>Cu<sub>0.5</sub>)Fe<sub>2</sub>O<sub>4</sub> Nanoparticles for Alcohol Amination under Microwave Heating. *ChemCatChem* 11, (2019), 3959

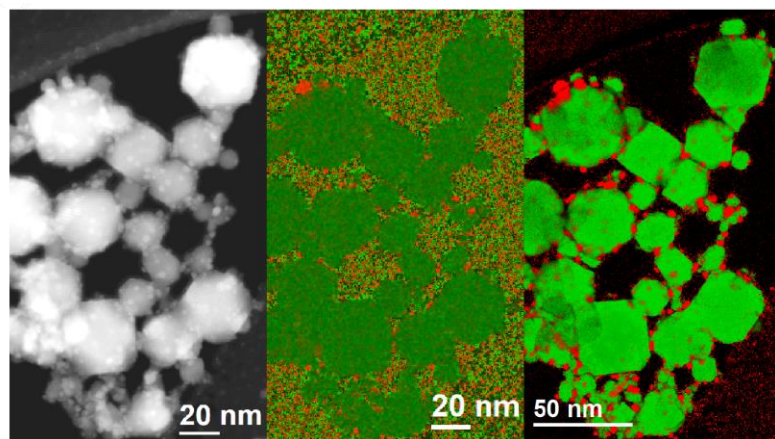


Figure 1. A) Scanning-TEM image of (Cu,Ni)-ferrites decorated with Cu<sub>0</sub> B) EELS elemental distribution computed with standard windowing methods (red = Cu, green = Ni+Fe) C) EELS elemental distribution with hierarchal multivariate statistics methods [3].

# Data-Driven Electron Microscopy Reveals Shape-Dependent Subpercent Strains in Gold Nanorods

Kohei Aso<sup>1\*</sup>, Jens Maebe<sup>2</sup>, Xuan Quy Tran<sup>3</sup>, Tomokazu Yamamoto<sup>4</sup>, Yoshifumi Oshima<sup>1</sup>, and Syo Matsumura<sup>3,4</sup>

<sup>1</sup> School of Materials Science, Japan Advanced Institute of Science and Technology, Asahidai 1-1, Nomi, Ishikawa, 923-1292, Japan

<sup>2</sup> Faculty of Sciences, Ghent University, Krijgslaan 281-S2, 9000 Ghent, Belgium

<sup>3</sup> Department of Applied Quantum Physics and Nuclear Engineering, Kyushu University, Motoooka 744, Nishi-ku, Fukuoka 819-0395, Japan

<sup>4</sup> The Ultramicroscopy Research Center, Kyushu University, Motoooka 744, Nishi-ku, Fukuoka 819-0395, Japan

\*aso@jaist.ac.jp

In nanomaterials, the physical properties are sensitive to the shape due to the large surface-to-volume ratio. The strain distribution in the nanoparticles with anisotropic shape has been expected to be non-uniform. However, such experimental results have not been reported so far, which is probably because of a lack of precision in strain analysis. In this study, we established a method to estimate the strain distribution of gold (Au) rod precisely from the atomic-resolution scanning transmission electron microscopy (AR-STEM) images by data-driven analysis and clarified the relationship between strain distribution and the shape of Au nanoparticles.

We observed three Au nanoparticles of 9 nm in diameter but different rod lengths (9 nm, 21 nm, and 36 nm) including a sphere by AR-STEM. Figure 1a shows a nanorod with a length of 21 nm. The ten images acquired with fast scan (1  $\mu$ s/pixel) were integrated into one image, to minimize both the effect of noise and instability of equipment.

Inter-columnar distances were measured from the AR-STEM images. The raw data from the core region surrounded with a rectangle in Fig. 1 contained noise components of random fluctuations up to  $\sim 1.2$  %. The Gaussian process regression (GPR) was applied to remove the noise components and the precision in local strain analysis was improved to 0.2 %.

We found that the rod-shaped nanoparticle had peculiar local strain distribution. Figure 2 shows a map of the strain of the (001) lattice spacing for the Au rod and sphere, where the (001) lattice is perpendicular to the horizontal direction in Fig. 2. In the case of the spherical particle (Fig. 2a), the lattice shows contraction near the surface (dark blue on the map), which is reasonable because of surface contraction. On the other hand, a lattice expansion (bright yellow on the map) of  $\sim +0.6\%$  was discovered near the tip of the rod-like nanoparticle (Fig. 2b) [1,2].

## References:

[1] K. Aso, *et al.*, *Microscopy*, Vol. 65 (2016), page 391–399

[2] K. Aso, *et al.*, *ACS Nano*, Vol. 15 (2021), page 12077–12085

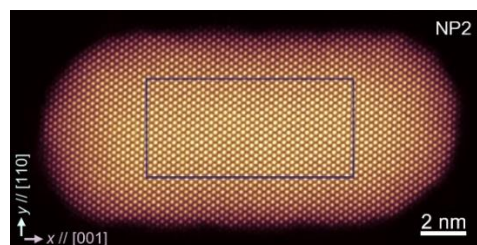


Fig. 1 AR-STEM image of a nanorod.

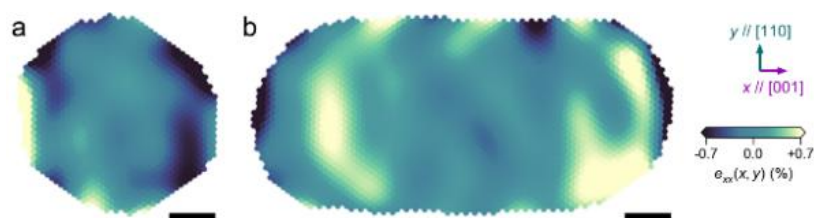


Fig. 2 Strain  $e_{xx}(x,y)$  maps of (a) a sphere and (b) the rod. Scale bars are 2 nm.

## Mapping electrostatic potential gradient in GaN NW *p-n* junctions using electron holography.

Anitha Jose<sup>1\*</sup>, Alex Mingze Yang<sup>1</sup>, Qihua Zhang<sup>2</sup>, Songrui Zhao<sup>2</sup>, and Karen L. Kavanagh<sup>1</sup>

<sup>1</sup> Department of Physics, Simon Fraser University, Burnaby, British Columbia V5A 1S6, Canada.

<sup>2</sup> Department of Electrical and Computer Engineering, McGill University, Montreal, Québec, H3A 0E9, Canada.

\*anithaj@sfu.ca

GaN nanowires (NWs) have been applied in devices including light emitting diodes (LEDs) [1], photodetectors [2] and laser diodes [3]. Understanding and controlling dopant incorporation is crucial for improving device performance. However, precise measurement of the dopant distribution in devices has been a difficult task [4]. Electron Holography (EH) is a technique that allows the quantitative determination of the electrostatic potential in a material [5] and therefore gives us a better understanding of the actual doping in the system.

We report the characterization of GaN nanowire (NW) axial *p-n* junctions by quantifying the built-in voltage and depletion width using off-axis EH. NWs were grown by Molecular Beam Epitaxy using Si and Mg as the n-type and p-type dopant respectively ( $N_D = 10^{18} \text{ cm}^{-3}$  and  $N_A = 10^{19} \text{ cm}^{-3}$ ). SEM image of the NWs showed a clear change in contrast suggesting the presence of a junction. The junction position was 200 nm from the top. Fig 1 (c) shows a longitudinal profile from the reconstructed phase image in (a), detecting an increase in phase from the p to n region. The corresponding potential profile estimated a built-in voltage ( $V_{bi}$ ) of  $1.0 \pm 0.1$  at the junction, assuming a hexagonal model. The depletion width was found to be  $31 \pm 2$  nm. The values of  $V_{bi}$  obtained from different NWs ranged from  $1.5 \pm 0.2$  V to  $0.9 \pm 0.1$  V. No stacking faults were detected as shown in BF TEM in (b). The expected  $V_{bi}$ , assuming 100% activation is 3.2 V. More experiments are underway to measure  $V_{bi}$  as a function of different dopant concentrations.

References:

[1] C.-Y. Chen et al, ACS Nano, 6, (2012), 5687-5692.

[2] X. Zhang et al, J. Mater. Chem. C, 5, (2017), 4319-4326.

[3] J. Heo et al, Appl.Phys. Lett., 98, (2011), 21110.

[4] Wallentin et al, J. Mater. Res., 26, (2011), 2142.

[5] M. Lehmann and H. Lichte, Microscopy and Microanalysis, 8, (2002), 447.

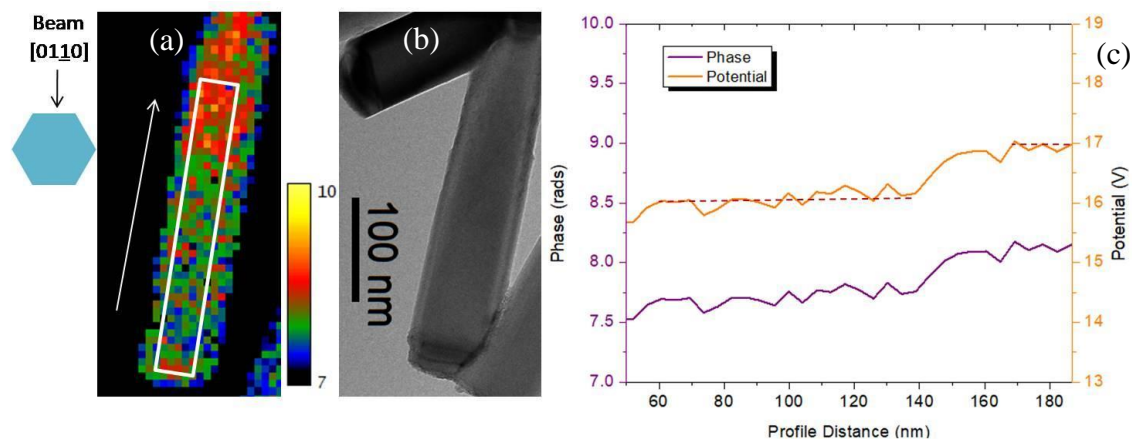


Figure 1: (a) Phase and (b) BF image with (c) a corresponding phase and potential profiles along the length of the wire. The profiles are an average within the white box in (a).

## Capturing the moment of nucleation and tracing the crystal growth by SMART-EM

Takayuki Nakamuro<sup>1\*</sup>, Masaya Sakakibara<sup>1</sup>, Hiroki Nada<sup>2</sup>, Koji Harano<sup>1</sup>, Eiichi Nakamura<sup>1</sup>

<sup>1</sup> Department of Chemistry, The University of Tokyo, Tokyo 113-0033, Japan.

<sup>2</sup> Environmental Management Research Institute, National Institute of Advanced Industrial Science and Technology (AIST), Tsukuba 305-8569, Japan

\*muro@chem.s.u-tokyo.ac.jp

Crystallization is essentially a stochastic process, and experimental studies of the mechanism have been difficult. Our research group has been developing a molecular electron microscopy technique called "single-molecule atomic-resolution time-resolved electron microscopy (SMART-EM)<sup>1</sup> imaging," which allows us to record the dynamic behavior of individual small molecules, as well as of molecular assemblies. In this study, by combining the SMART-EM imaging method with a newly developed sample preparation method, we have succeeded in continuously imaging and analyzing the process of spontaneous assembly of sodium chloride (NaCl) molecules to form crystal nuclei and then grow into crystals.<sup>2</sup>

We captured the moment when NaCl crystal nuclei of about 1 nm in size repeatedly formed at the tip of the carbon nanohorn (CNH), and it became clear that the pre-nucleation molecular aggregates were moving back and forth between a crystal-like ordered structure and a disordered structure by disassociation and aggregation (Figure 1) Details of this mechanism will be discussed in the presentation.

In summary, we developed a new microscopy technique for the common phenomenon of crystallization (Figure 2), and analyzed the mechanism at the molecular level.

### References:

[1] E. Nakamura, *Acc. Chem. Soc.* **2017**, *50*, 1281–1292.

[2] T. Nakamuro, M. Sakakibara, H. Nada, K. Harano, E. Nakamura, *J. Am. Chem. Soc.* **2021**, *143*, 1763–1767.

### A Crystal Emerges from a Chaotic Sea of Molecules

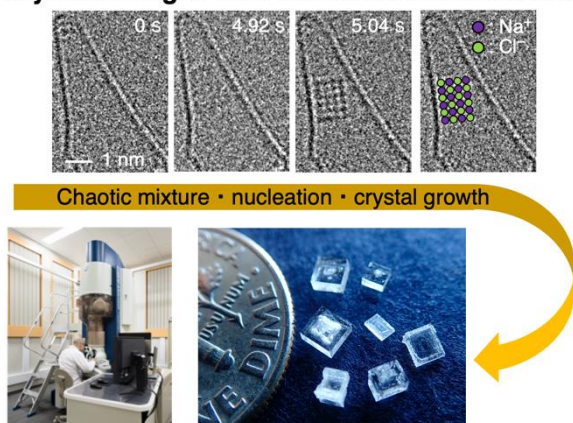


Fig. 1 Summary: TEM observation of NaCl units aggregating into crystals at the tip of a CNH.

結晶ができる瞬間をカメラで捉えた！  
Capturing the moment of crystallization!



Fig. 2. YouTube links to videos related to this presentation.

## Phase Imaging Electron Intensities on the Diffraction Plane

Rodney A Herring, MENG, CAMTEC, University of Victoria, Victoria, B.C. Canada V8W 2Y2

A method to interfere electron intensities on the diffraction plane invented during the Tonomura Electron Wavefront Project [1], somewhat surprisingly, reveals all sources of intensity, i.e., elastically and inelastically scattered, have sufficient coherence to form fringes enabling the measurement of their phases. For example, using the self-interference of elastically-scattered HOLZ line intensities was used to measure the three-dimensional strain distribution through the crystals making it possible to solve the Howie-Whelan equation [2, 3]. Interfering symmetric Bragg diffraction beams measured the strain profile at dislocation cores where the  $2\pi$  phase shift produces a physical singularity at its center, possibly the smallest in existence [4]. More recent observations revealed residual two dimensional lattice phase images where a flat phase image was expected possibly due to dynamic diffraction, Fig. 1 [5]. If true, dynamic diffraction can be studied as a function of specimen thickness, diffracted beam extinction distances and deviation parameter from exact Bragg diffraction. These studies will be presented for discussion during the workshop.

### References

1. Tonomura Electron Wavefront Project (1989 – 1994), Exploratory Research for Advanced Technology (ERATO), Japan Science and Technology Corporation, Kawaguchi Center Bldg., 4-1-8, Honcho, Kawaguchi-shi, Saitama 332 Japan.
2. Herring, R.A., M. Norouzpour, K. Saitoh, N. Tanaka, and T. Tanji, “Determination of three-dimensional strain state in crystals using self-interfered split HOLZ lines” *Ultramicroscopy* 156 (2015) 37-40.
3. Norouzpour, M. and R.A. Herring, “Aberration-corrected self-interference of split higher order Laue zone Line for measuring the z-dependent strain profile” *J. Mater. Res.*, Vol. 32, No. 5, (2017) 996 – 1008.
4. Herring, R.A., “Phase Imaging Dislocations using Diffracted Beam Interferometry” *Microscopy* (2020) MICRO-2020-00047.
5. Herring, R.A., “Dynamic Diffraction Lattice Phase Imaging Using DBI” *Microsc. Microanal.* 27 (Suppl 1), (2021) 2194/5.

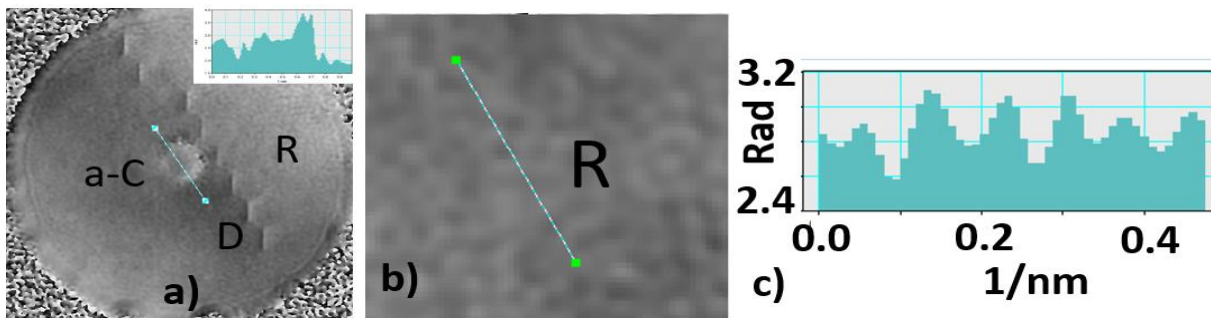


Fig. 1 – a) DBI phase image of the interference of symmetrical Bragg diffracted beams of Au showing an amorphous C (a-C) deposit with its phase spectrum passing through the line in the upper right corner, a dislocation network at D and the residual phase, R, in the perfect crystal magnified in b) and its phase spectrum along the line shown in c) clearly revealing the complex phase shift's periodicity.

# Application of 4D-STEM at 30 kV for structure analysis of block co-polymers and high-resolution multi-slice phase retrieval

Arthur M. Blackburn<sup>1\*</sup>, Cristina Cordoba<sup>1</sup>, Robert McLeod<sup>2</sup>, Yifan Zhang<sup>1</sup> and Ian Manners<sup>1</sup>

<sup>1</sup> University of Victoria, 3800 Finnerty Road, Victoria, BC, V8W 2Y2, Canada

<sup>2</sup> Hitachi High-Tech Canada Inc., 89 Galaxy Blvd, Etobicoke ON, M9W 6A4, Canada

\*ablackbu@uvic.ca

Scanning transmission electron microscopy (STEM) at 30 kV combined with low angle annular dark field (LAADF) detection can provide strong in-focus image contrast on weak contrast polymer materials. In comparison to higher beam energy TEM, it offers some stronger beam-sample interactions and may reduce some beam induced damage mechanisms. Furthermore, 30 kV STEM imaging can be performed in SEM class instruments which generally offer greater ease of use and reduced cost. In this work we integrated a high-speed direct detection camera to a SEM type instrument (Hitachi SU9000), to enable the rapid collection of low-dose four dimensional (4D)-STEM data sets, where a diffraction pattern is collected at each scanned position. This is exemplified here with the collection of 10000 diffraction patterns (DPs), each with a 10 ms exposure from a  $20 \times 20 \mu\text{m}$  field of view, to yield a non-sample destructive average electron dose of  $17 \text{ e}^-/\text{\AA}^2$ . These conditions provided new insights into the structural origins of branching within specific block co-polymers [1], an example of which is in Fig. 1a. Here DPs (Fig 1b, c) obtained from the central and branch regions differ, indicating an additional nucleation site at the branch point.

Additionally, we show 4D-STEM data sets obtained in this instrument, using only simple projection optics, can be processed using multi-slice ptychographic algorithms to allow 50 pm (or better) features to be resolved at 30 kV (Fig 2a, b). Though electron ptychography was first experimentally demonstrated at 30 kV [2] showing 236 pm lattice fringes, relatively little exploration of ptychography at this energy has been pursued since then, particularly with the direct electron detectors, such as the one used in this work (Dectris Quadro). We thus summarize that a high-speed pixelated direct electron detector on a low kV SEM/STEM instruments provides great utility in the structural characterization of dose sensitive materials and provides access to high-resolution phase imaging through ptychography.

[1] Y. Zhang, S. Pearce, *et al.*, J. Am. Chem. Soc., Vol. 143, (2021), 5805-14.

[2] M. J. Humphry, B. Kraus, *et al.*, Nature Comms., Vol.3, (2003), 730.

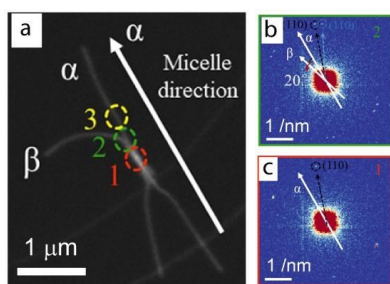


Fig. 1 (a) LAADF image of a typical branched block co-polymer, where (b) a DP collected from the branching region shows dual patterns and (c) the central region DP shows a single pattern.

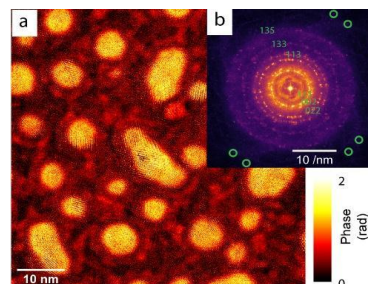


Fig. 2. (a) Reconstructed phase (30 kV) of gold particles on carbon film from ptychography and (b) its FFT, with strong diffraction ring indices labelled and 50 pm peaks encircled.

## Visual Molecular Science at Interface of Self-Assembly and Electron Microscopy

Koji Harano<sup>1\*</sup>

<sup>1</sup> Department of Chemistry, The University of Tokyo, 7-3-1, Hongo, Bunkyo-ku, Tokyo, 113-0033, Japan.

\*harano@chem.s.u-tokyo.ac.jp

It remains as a challenge to design functions of self-assembled materials in a predictable manner because of the lack of understanding on self-assembly processes at a molecular level. We have developed new electron microscopic methods named single-molecule atomic-resolution time-resolved electron microscopy (SMART-EM) that provides information on the time evolution of the structures of individual molecules and self-assembled molecules. The key is that we observed little sign of decomposition of the specimen molecules encapsulated in or attached to a single-walled carbon nanotube (CNT) as opposed to solid organic materials. The high specimen stability and the real-time movie recording enable us to study on the conformation of  $^{13}\text{C}$ -each carbon-carbon bond in single perfluoroalkyl fullerene molecules, dynamic conformational changes of linear molecules, and structure of organic nanoclusters formed as a precursor of a crystal nucleus from supersaturated solution. Recently we have demonstrated that the SMART-EM video imaging provides a unique methodology for capturing and analyzing the minute reaction intermediates, as illustrated for new host-guest binding modes of cyclodextrins (Fig. 1) and prenucleation clusters in the reaction mixture of metal-organic frameworks (Fig. 2). In this lecture, I would also like to discuss the significance of in-situ observation of individual molecules in chemical events using the high-speed molecular video imaging.

References: *Nat. Mater.* **11**, 877–881 (2012). *J. Am. Chem. Soc.*, **136**, 466–473 (2014). *J. Am. Chem. Soc.*, **137**, 3474–3477 (2015). *J. Am. Chem. Soc.*, **139**, 18281–18287 (2017). *Nat. Commun.*, **10**, 3608 (2019). *Bull. Chem. Soc. Jpn.* **93**, 1079–1085 (2020). *Bull. Chem. Soc. Jpn.* **93**, 1603–1608 (2020). *Microsc. Microanal.* **26**, 667–675 (2020). *J. Am. Chem. Soc.* **143**, 1763–1767 (2021). *J. Am. Chem. Soc.* **143**, 5786–5792 (2021). *ACS Nano* **15**, 12804–12814 (2021). *arXiv* 2107.01490.

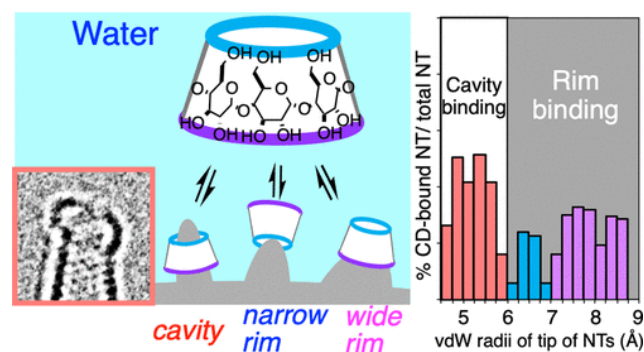


Fig. 1 Statistic TEM image analysis of cyclodextrins bound to spherical tips of carbon nanotubes, demonstrating the existence of a rim binding mode in addition to the conventional cavity binding to cyclodextrins.

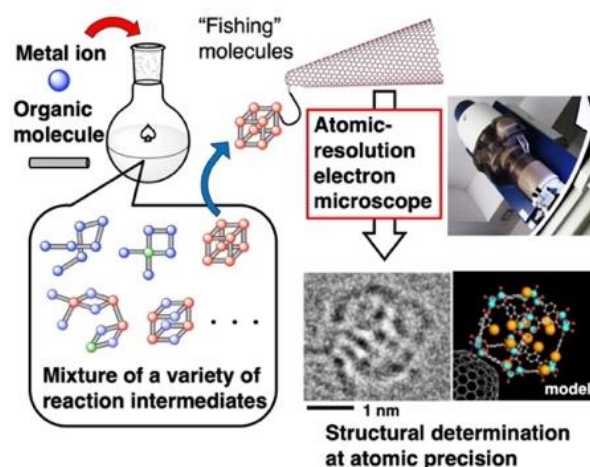


Fig. 2. Capturing and TEM imaging of reaction intermediates from a mixture of metal-organic framework synthesis by using a chemically-functionalized carbon nanotubes as “fishhook” for a nucleating cluster.

# Contribution of microstructure in oblique impact morphology of high entropy CrMnCoFeNi particles

Roghayeh Nikbakht \*

Mechanical engineering Department, University of Ottawa, Ottawa, ON, Canada

[roghayeg.nikbakht@uottawa.ca](mailto:roghayeg.nikbakht@uottawa.ca)

Cold spray is a powder consolidation method at which micron size particles are accelerated to high velocities (300-1200 m/s) and deposit to a substrate as a result of plastic deformation and native oxide removal [1, 2]. Microstructure of powder particles plays an important role in oblique impact morphology. In this study CrMnCoFeNi high entropy alloy (HEA) particles were sprayed on Nickel substrates using Helium as a process gas (3.2 MPa and 400 °C). The morphology and microstructure of the single particles were analyzed using tilted view SE images, electron channelling contrast imaging (ECCI) (EVO MA-10, Carl Zeiss), and EBSD analyses (SU-8230 Hitachi cold field emission).

A gas atomized spherical CrMnCoFeNi powder with a cellular structure is used for single-particle experiments (Fig. 1(a)). The ECCI maps of the cross-sections of two powder particles show two different morphologies: one with elongated grains and one with relatively equiaxed structure (Fig. 1(a1) and (b1)). The deformed particles morphology change from perfect half-sphere with jetting zones located at the lips (Fig.1(a2)), to half sphere morphology with some protuberances in the rim of the half-sphere (Fig.1(b2)). ECCI maps and IPF maps of two CrMnCoFeNi particles in Fig. 1(a2-a3) with an equiaxed grain distribution presents a symmetrical half-sphere impact morphology while the particle of Fig. 1(b2-b3) with elongated morphology deviates from symmetrical half-sphere morphology and is closer to a top-hat morphology. KAM maps (Fig. 1(a4-b4)) demonstrate a higher degree of misorientation at grain boundaries of elongated grains which implies that grain boundaries are involved in the variation of particle impact morphologies by affecting the mechanism of plastic strain transfer or slip transfer (transmission) between particle grains. The generated dislocations at the lower part of the particles can move easily inside the elongated grains –or toward the free surface of the particle in this case - without being forced to transmit to the neighbouring grains (see Fig 1 (b4)). Microstructure variation of powder particles may result in different impact physics and ultimately impact morphology.

## References:

- [1] R. Nikbakht, S.H. Seyedein, S. Kheirandish, H. Assadi, B. Jodoin, Asymmetrical bonding in cold spraying of dissimilar materials, *Appl. Surf. Sci.* 444 (2018) 621-632.
- [2] R. Nikbakht, H. Assadi, B. Jodoin, Intermetallic Phase Evolution of Cold-Sprayed Ni-Ti Composite Coatings: Influence of As-Sprayed Chemical Composition, *J. Therm. Spray Technol.* 30 (2021) 119–130
- [3] R. Nikbakht, M. Saadati, H. Assadi, K. Jahani., and B. Jodoin, Dynamic microstructure evolution in cold sprayed NiTi composite coatings, *Surf. Coat. Technol.* (2021) 421, p.127456.

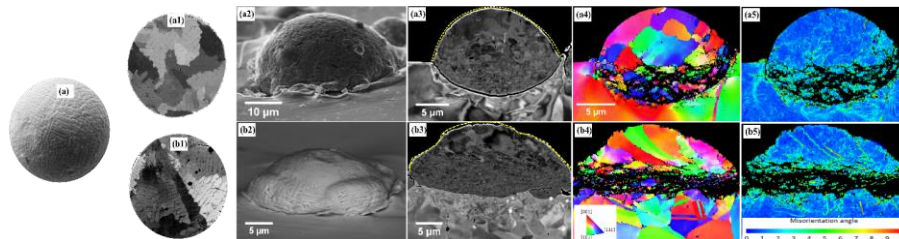


Figure 1. Effect of particle microstructure on impact morphology. (a) morphology of powder particle, (a1-b1) ECCI maps of cross-section of CrMnCoFeNi alloy particles, (a2-b2) morphology of deposited particle, (a3-b3) ECCI map of cross-section of particles, (a3-b3) IPFs maps and (a5-b5) KAM maps.

# Atomic bond stiffness in Pt atomic chains measured by TEM coupled with a quartz LER

Yoshifumi Oshima<sup>1\*</sup>, Jiaqi Zhang<sup>1</sup>, Masahiko Tomitori<sup>1</sup>

<sup>1</sup> Japan Advanced Institute of Science and Technology (JAIST), 1-1 Asahidai, Nomi, 923-1292, Japan.

\*oshima@jaist.ac.jp

Monatomic chains have shown unique physical and chemical properties, which draws a different picture from their bulk counterparts. It has been reported that the electrical or magnetic properties can be tuned by controlling the length of the atomic chains, which indicate that the mechanical properties is very important for their applications. However, the mechanical properties of atomic chains have not been clarified experimentally. To solve this problem, we developed an in-situ TEM holder equipped with a quartz resonator as force sensor (Fig. 1a) [1] to measure the mechanical properties of atomic chains when observing their atomic configurations.

A quartz length-extension resonator (LER) was used to measure the stiffness of platinum (Pt) monatomic chains from its frequency shift. Because the stiffness of the atomic chain suspended between the edge of LER and the fixed counter base can be measure precisely with very small oscillation amplitude (about 30 pm). The atomic resolution TEM images (Fig. 1b) and videos were captured simultaneously with measuring the conductance and stiffness by our developed TEM holder.

The stiffness of atomic chains with 2-5 atoms were obtained (Fig. 1c). By subtracting the stiffness of the electrodes supporting the monatomic chain from the measured stiffness, we found that the stiffness of a Pt monatomic chain varied with the number of the constitute atoms in the chain. We investigated the stiffness of about 150 Pt monatomic chains for reproducibility and confirmed that the middle bond stiffness (25N/m) in the chain was slightly higher than that of the bond connect to the suspending tip (23N/m). In addition, the maximum elastic strain of individual bond in the chain was as large as 24% [2]. These values were obviously different from the bulk counterpart. Such peculiar values could be briefly explained by the concept of “string tension”.

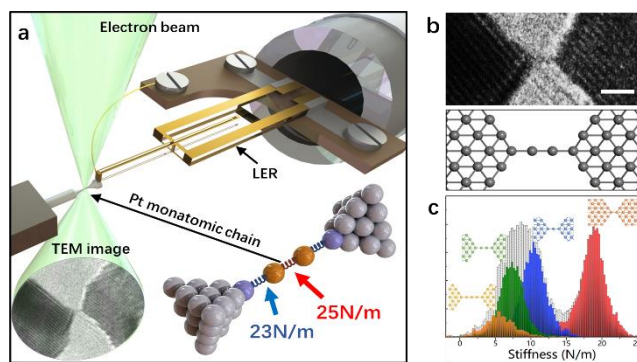


Fig. 1. (a) Schematic illustration of the experimental setup. (b) TEM image of an atomic chain with 4 atoms and corresponding atomic configurations of the chain. (c) Stiffness histograms of the Pt monatomic chains.

## References

[1] J. Zhang et al, *Nanotechnology*. 31 (2020) 205706.

[2] J. Zhang et al, *Nano letters*. 21 (2021) 3922-3928.

## Thermal Evolution of Alloying State in Ternary IrPdRu Nanoparticles

Xuan Quy Tran<sup>1\*</sup>, 山本知一 (Tomokazu Yamamoto)<sup>2</sup>, 松村 晶 (Syo Matsumura)<sup>1,2</sup>  
草田康平 (Kohei Kusada)<sup>3</sup>, 吴冬霜 (Dongshuang Wu)<sup>3</sup>, 北川 宏 (Hiroshi Kitagawa)<sup>3</sup>

<sup>1</sup> Department of Applied Quantum Physics and Nuclear Engineering, Kyushu University, Motoooka 744, Nishiku, Fukuoka 819-0395, Japan.

<sup>2</sup> The Ultramicroscopy Research Center, Kyushu University, Motoooka 744, Fukuoka 819-0395, Japan.

<sup>3</sup> Department of Chemistry, Kyoto University, Kitashirakawa-Oiwakecho, Kyoto 606-8502, Japan

\*tran.xuan.quy.044@m.kyushu-u.ac.jp

Compositional and structural arrangements of constituent elements, especially those at the surface and near-surface layers, greatly influence the catalytic performance of alloyed nanoparticles (NPs). The compositional stability and associated structural evolution of a ternary Iridium–Palladium–Ruthenium (IrPdRu) nanoalloy at elevated temperatures have been studied using interrupted *in-situ* scanning transmission electron microscopy and theoretical modeling [1].

Equiatomic solid-solution nanoalloys of IrPdRu were synthesized *via* a modified polyol method where the metal precursors ( $K_2PdCl_4$ ,  $RuCl_3 \cdot nH_2O$ , and  $IrCl_4 \cdot nH_2O$ ) dissolved in deionized water were added to a triethylene glycol solution heated at 230 °C using PVP as a protecting agent. The NP samples were dispersed in ethanol and were dropcasted onto the carbon-supported membranes of MEMS E-chips. Structural analysis was performed on a JEOL JEM-ARM200CF operated at 200 kV with an Aduro heating holder (Protochips). Canonical Monte Carlo (MC) simulations were performed for a NP model containing  $N = 5,793$  atoms ( $\sim 5.6$  nm in size) based on the Metropolis algorithm to gain atomistic insights of the compositional evolution. The total energy of the model during the MC simulations was continuously evaluated using the molecular dynamics library LAMMPS and our developed EAM potential for IrPdRu.

Figure 1 tracks compositional time-evolution of IrPdRu NPs annealed at 500 °C using composite XEDS maps and the corresponding Gibbs triangles [2]. In the latter, the center of the compositional profiles slightly displaces from the original position toward the Ir-Ru edge. In a NP model given in Fig. 2, there is a cumulative coverage of Pd atoms in the surface, while Ir and Ru atoms remain mixing in the core region, shifting the composition center in the Gibbs triangle in a similar manner as in Fig. 1.

References:

[1] X. Q. Tran, *et al.*, *ACS Nano*, submitted for publication

[2] X. Q. Tran, *et al.*, *J. Phys. Chem. C*, **124** (2020), 21843.

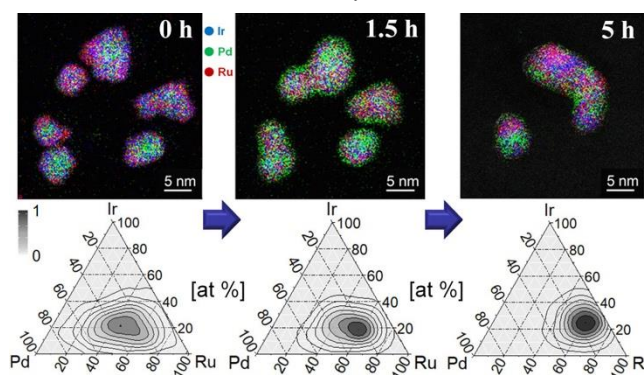


Fig. 1. Tracking the sub-nm compositional evolution in a IrPdRu particle cluster annealed at 500 °C in terms of XEDS maps and corresponding Gibbs composition triangles.

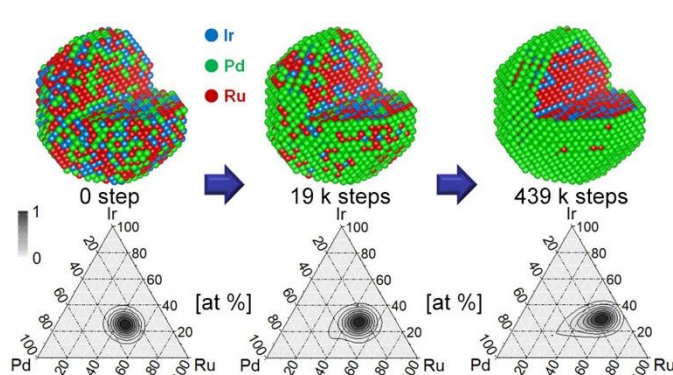


Fig. 2. Canonical MC simulations for a IrPdRu particle model ( $\sim 5.6$  nm) at 500 °C, and Gibbs triangle representation of the local compositional sampled from 2D pixel columns of  $0.7 \times 0.7 \times l$  nm<sup>3</sup>.

## Utilization of Correlative Light and Electron Microscopy for Analyzing the Structural Organization of Bacterial Microcrystalline Cellulose

Alyssa Williams<sup>1</sup>; Mouhanad Babi<sup>2</sup>; Marcia Reid<sup>4</sup>; Kathryn Grandfield<sup>1,3</sup>; Nabil Bassim<sup>1,3,4</sup>; Jose Moran-Mirabal<sup>2,5</sup>

<sup>1</sup>School of Biomedical Engineering, McMaster University, Hamilton, ON, Canada

<sup>2</sup>Department of Chemistry and Chemical Biology, McMaster University, Hamilton, ON, Canada

<sup>3</sup>Department of Materials Science and Engineering, McMaster University, Hamilton, ON, Canada

<sup>4</sup>Canadian Center for Electron Microscopy, McMaster University, Hamilton, ON, Canada

<sup>5</sup>Centre for Advanced Light Microscopy, McMaster University, Hamilton, ON, Canada

Cellulose's mechanical strength and bioavailability have contributed to its prominent use in industrial applications where it undergoes biochemical processing including depolymerization [1]. In the cellulose microfibril structure, disordered regions or "dislocations" along the fibril have been characterized as key sites for cellulose degradation [2]. In this correlative light and electron microscopy (CLEM) workflow, the specificity and localization precision of super-resolution imaging (SR) and the nanoscale high-resolution imaging from transmission electron microscopy (TEM) were used to investigate and elucidate ultrastructural details of the bacterial microcrystalline cellulose (BMCC) microfibril structure. For CLEM imaging, a sample preparation method has been adapted, where Cy5 labelled BMCC microfibrils were prepared on TEM alphanumeric finder grids with imaging buffer and placed in between coverslips for direct stochastic reconstruction microscopy (dSTORM), an SR imaging technique, using a Leica DMI6000 B microscope (Fig 1.a)) [3]. Due to the accessibility of dislocation areas on the microfibrils, Cy5 binds and aggregates in these regions. Thereby, indicating the presence of a dislocation on the microfibril. BMCC microfibrils of interest were identified from the dSTORM images and located on the finder grid. The TEM grids were then washed and dried to be made vacuum compatible for TEM imaging. BMCC microfibrils were identified and imaged at the nanoscale in bright field TEM imaging on a JEOL JEM 1200EX TEMSCAN microscope (Fig 1.b)). Adobe photoshop was utilized to overlay SR and TEM images (Fig 1.c)). Analysis of composite image revealed that dislocation areas (bright Cy5 spots) on the BMCC microfibril appear to overlap with fibril twisting regions (darker regions).

### References:

- [1] Lynd et al., *Microbiol Mol Biol Rev*, Vol. 66, (2002), 506-577.
- [2] Hidayat et al., *Cellulose*, Vol. 19, (2012), 1481–1493.
- [3] van Elsland et al., *Chembiochem*, Vol. 19, (2018), 1766-1770.

## **Manual versus automatic analysis of microglial spatial characteristics: a comparison in the hippocampus of healthy adult mice**

Mohammadparsa Khakpour<sup>1</sup>, Fernando González Ibáñez<sup>2</sup>, Maude Bordeleau<sup>2,3</sup>, Laura Maggi<sup>4</sup>, Marie-Ève Tremblay<sup>1-3,5-6</sup>

Corresponding author email: Parsa.khakpour2000@gmail.com

<sup>1</sup> Division of Medical Sciences, University of Victoria, Victoria, BC, Canada; <sup>2</sup> Axe Neurosciences, Centre de recherche du CHU de Québec-Université Laval, Québec, QC, Canada; <sup>3</sup> Neurology and Neurosurgery Department, McGill University, Montréal, QC, Canada; <sup>4</sup> Department of Physiology and Pharmacology, Istituto Pasteur-Fondazione Cenci Bolognetti, Sapienza University of Rome, Rome, Italy; <sup>5</sup> Department of Molecular Medicine, Université de Laval, Québec City, QC, Canada; <sup>6</sup> Department of Biochemistry and Molecular Biology, University of British Columbia, Vancouver, BC, Canada;

Image analysis is a powerful tool in neuroscience. Many approaches in image analysis still depend on manual identification and tracking of biological events. This manual approach can introduce personal bias and require long sessions of work. Automatization of analytical processes represents a potential solution for bias and time investment. Methods that optimize the analysis quality by increasing efficiency and reducing bias are favored. To establish such a methodology, a micro command was developed that runs on ImageJ to apply image analysis. However, the provided micro command requires to be validated and compared with the manual analysis to assess the performability of automatic analysis for microglia research. Microglia are immune cells found throughout the brain parenchyma. Recent studies suggested that microglial spatial characteristics (e.g. density) are not homogeneous between different brain regions. Microglial spatial characteristics analysis provides valuable information on their various functions. Manually recognizing individual cells is the subject of time-consumption and bias. The script performs microglial cell body selection in brain regions that are manually traced for the spatial analysis. The main core of the micro script consists of four sections. The script involves the cell selection assessment and executes automatic spatial analysis for each individual cell. The data generated with this workflow provides spatial characteristics measurement. The current study focused on comparing manual versus automatic analysis directly to found out whether the automatic analysis is efficient enough to replace the manual analysis. The command is a groundbreaking instrument that reduces the analysis time length, produces valid data, and decreases the sensitivity to possible bias.

## Belief theory enables detection of Caveolae in superresolution microscopy.

Ben Cardoen<sup>1\*</sup>, Timothy Wong<sup>2</sup>, Ivan Robert Nabi<sup>2\*\*</sup>, Ghassan Hamarneh<sup>1\*\*</sup>

<sup>1</sup> Medical Image Analysis Research Group, Simon Fraser University, British Columbia, Canada

<sup>2</sup> Department of Cellular and Physiological Sciences, Life Sciences Institute, University of British Columbia, British Columbia, Canada

\*[bcardoen@sfu.ca](mailto:bcardoen@sfu.ca)

\*\* Equal contribution

Supported by CIHR grants PJT-159845, PJT-156424 and PJT-175112

We developed a novel method[1] that enables the automatic detection of CAV1 structures in STED super resolution microscopy.

Our method detects objects automatically across images with varying intensity profiles, then uses the cell level label to build a model that identifies which objects are discriminating for each cell type. Our model leverages belief theory to automatically learn a per object label, with lower and upper bound probabilities, including the uncertainty in identification of each object. We identify Caveolae and scaffolds, two types of CAV1 protein complexes, that are key to preventing membrane breakage of the cell membrane in response to stress. Our results match identification of CAV1 structures in fixed cells imaged using dSTORM[2]. Our STED based method enables the detection in live cells, where the formation dynamics can be observed and extracted.

References:

[1] Cardoen, B., Wong, T., Alan, P., Lee, S., Matsubara, J.A., Nabi, I.R. and Hamarneh, G., 2020. SPECHT: Self-tuning Plausibility Based Object Detection Enables Quantification of Conflict in Heterogeneous Multi-scale Microscopy.

[2] Khater, Ismail M., Qian Liu, Keng C. Chou, Ghassan Hamarneh, and Ivan Robert Nabi. "Super-resolution modularity analysis shows polyhedral caveolin-1 oligomers combine to form scaffolds and caveolae." *Scientific reports* 9, no. 1 (2019): 1-10.

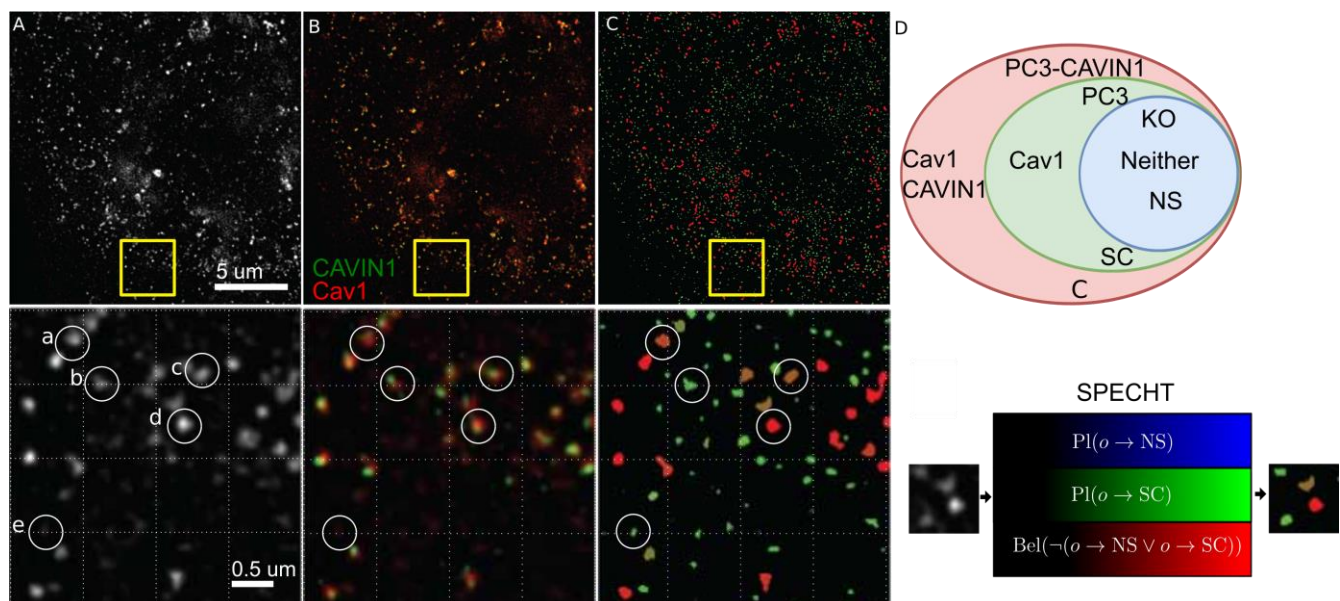


Figure 1: Identification of CAV1 protein complexes in STED superresolution microscopy. The identified Caveolae show the expected colocalization with Cavin1 (B). Our model uses 3 cell level labels to build its discriminatory capability (D). Figure based on original from [1].

## TEM/STEM Intensity Modulation with Increasing Thickness Induced by Electron Multiple Scattering Phenomena in Materials

山崎 順(Jun Yamasaki)<sup>1,2\*</sup>, 西久保 英郎(Hideo Nishikubo)<sup>3</sup>, 佐々木 宏和(Hirokazu Sasaki)<sup>3</sup>, 荒井 重勇(Shigeo Arai)<sup>2</sup>

<sup>1</sup> Research Center for Ultra-High Voltage Electron Microscopy, Osaka University, 7-1, Mihogaoka, Ibaraki, Osaka567-0047, Japan.

<sup>2</sup> Institute for Materials and Systems for Sustainability, Nagoya University, Japan.

<sup>3</sup> Furukawa Electric Co., Ltd., Japan. \* yamasaki@uhvem.osaka-u.ac.jp

Clarification of the thickness dependence of image contrast in transmission electron micrographs is important for deep understanding of multiple scattering phenomena of high-energy electrons as well as from the viewpoint of applications to various experiments, such as effective observations of thick samples including *in-situ* experiments and quantitative electron tomography [1]. In the present study, the image intensity in bright-field (BF-) TEM and ADF-STEM were analyzed for polystyrene, amorphous carbon, and amorphous NiP as functions of thickness [2].

Figure 1 shows examples of the results, which were measured in BF-TEM images of polystyrene taken with various beam energies. Contrary to the general understanding that the electron transmission  $T$  decreases exponentially with increasing thickness (shown by broken straight lines in the log plot in Fig. 1), the measured attenuations show curves attributed to multiple scattering phenomena [1, 2]. By analyzing all the data obtained under a wide range of conditions (acceleration voltage of 200 kV–3 MV, aperture acceptance angles of 0.85–30 nm<sup>-1</sup>, and thickness of 0.25–10 μm), it was found that they were expressed well by a function containing three parameters [2], as seen in the excellent fittings in Fig. 1. We succeeded in expressing the attenuation function approximately based on a simple mathematical model of the multiple scattering. Moreover, we found that also the thickness dependences of ADF-STEM intensity obtained with various detection angles were successfully expressed by simple extensions of the proposed function as shown in Fig. 2. The benefit to achieve quantitative electron tomography is also discussed.

References:

[1] J. Yamasaki, *et al.*, *Microscopy* **63**, 345 (2014).

[2] J. Yamasaki, Y. Ubata and H. Yasuda, *Ultramicroscopy* **200**, 20 (2019).

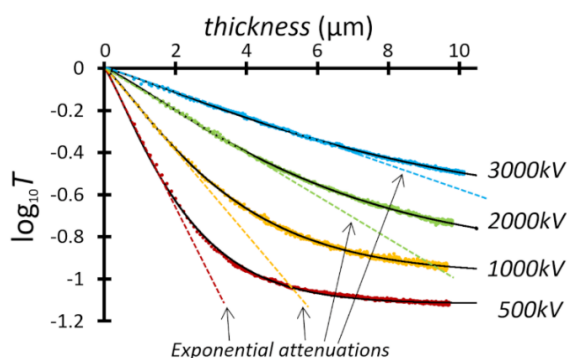


Fig. 1. Intensity attenuations in BF-TEM images of polystyrene taken with various acceleration voltages. All the data (color dots) are fitted well by the proposed function (solid curves).

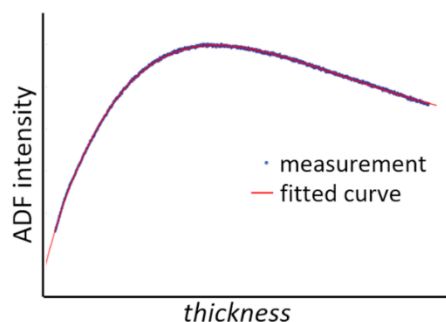


Fig. 2. ADF-STEM intensity of amorphous NiP taken with 1000 kV. The measured intensity (blue dots) are fitted well by the extension of the proposed function (red curve).

# NanoMi: a Public-License Platform for Electron Microscopy Development and Education

Marek Malac<sup>1,2\*</sup>, M. Kamal<sup>1</sup>, K. Kumar<sup>2</sup>, J. A. Marin-Calzada<sup>2</sup>, M. Salomons<sup>1</sup>, D. Homeniuk<sup>1</sup>, D. Vick<sup>1</sup>, R. Au<sup>2</sup>, A. Czarnecki<sup>2</sup>, D. Price<sup>1</sup>, M. Hayashida<sup>1</sup>, M. Cloutier<sup>1</sup>, R.F. Egerton<sup>2</sup>

<sup>1</sup> NRC-NANO, 11421 Saskatchewan Dr., Edmonton, T6G 2M9, Canada.

<sup>2</sup> Dept. of Physics, University of Alberta, Edmonton, T6G 2E1, Canada.

\*marek-malac@nrc-cnrc.gc.ca

We are developing a modular electron microscope column distributed under a public license [1,2], referred to as NanoMi. Elements of modeling and control software are already freely available [2]. The target for release of blueprints and circuit diagrams is late 2021.

NanoMi is intended to provide SEM, STEM, TEM and electron diffraction capabilities. NanoMi is based on electrostatic Einzel lens and operates at up to 50 kV. Electron-optical components are independent from the vacuum envelope, and are ultra-high vacuum (UHV) compatible. Fig. 1 shows a view of the NanoMi column internal arrangement. It is ~1300 mm tall in STEM / TEM configuration. SEM functionality can be implemented with ~500 mm column height. Fig 2. shows the current layout of the SEM probe-forming optics. Modeling suggests ~1000x source demagnification at the sample plane, providing ~30 nm probe when using a W-hairpin source. We are testing and debugging SEM and STEM hardware, electronics and software control. Simulation and control SW are written in Python and run on a single Linux PC.

NanoMi can be attached to an existing experimental apparatus, e.g. thin film growth system, to customize experiments. It can also provide a test bench for development of electron-optical components. The use of electrostatic electron-optics reduces NanoMi’s heat load, could increase the scan speed in SEM, and could allow the future use ions rather than electrons.

[1] M Malac et al. Microscopy and Microanalysis 26 (S2), (2020), 1810.

[2] NanoMi.org [osf.io/bpj73/](https://osf.io/bpj73/) [github.com/NRC-NANOmi/NanoMi](https://github.com/NRC-NANOmi/NanoMi)

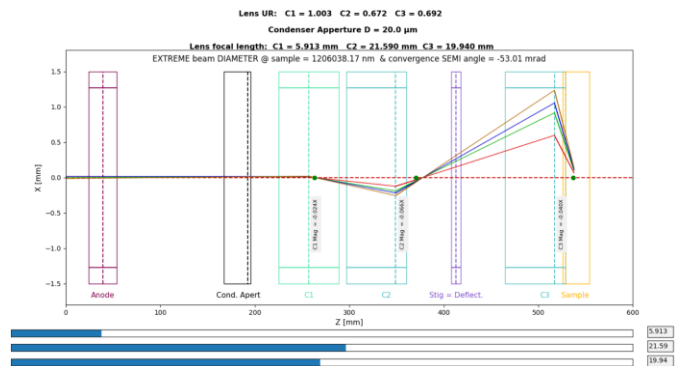
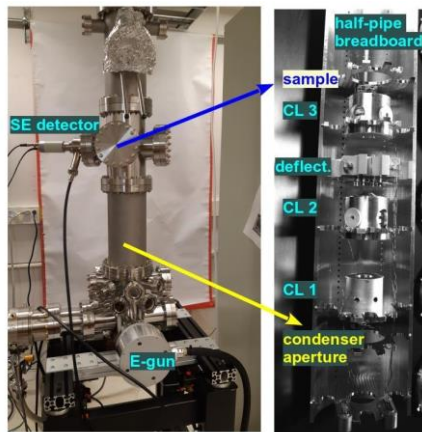


Fig. 1 Photo of the NanoMi column and the electron-optical “breadboard” of NanoMi. The electron source is located at the bottom. The use of a breadboard concept to mount optical elements allows for convenient optics modifications.

Fig. 2. Interactive matrix optics layout for SEM probe formation. Currently, NanoMi comprises of three Einzel-type condenser lens at 232, 382 and 509 mm from the electron source. The sample plane is located at 529 mm.

# STEM-Moiré Applications to Crystalline Specimens without using High-End Microscopes

Junji Yamanaka<sup>1\*</sup>, Chiaya Yamamoto<sup>1</sup>, Kosuke O. Hara<sup>2</sup>, Keisuke Arimoto<sup>2</sup>

<sup>1</sup> Center for Inst. Analysis, University of Yamanashi, 4-3-11 Takeda, Kofu, JAPAN

<sup>2</sup> Center for Cry. Sci. & Tech., University of Yamanashi, 7-32 Miyamae, Kofu, JAPAN

\*: jyamanak@yamanashi.ac.jp, corresponding author

Studies about STEM moiré, which is a moiré between scanning lines of STEM and crystal lattice, are progressing recently [1-4]. It is very useful to analyze lattice strains in semiconductor materials and it is expected to use for many other crystalline materials. Our group has been focusing on the usage of STEM moiré without using highly specified machines, because we think that may contribute to many researchers in the field of materials sciences [5, 6]. In this presentation, we will summarize and report our previous experimental results about STEM moiré.

A field-emission type STEM (FEI Tecnai Osiris) without any Cs correctors was utilized with an acceleration voltage of 200 kV in this study. We observed the STEM moiré between the incidental-electron scanning lines and the {111} planes of the Si, SiGe, and Ge. Fig. 1 shows STEM bright field image of the SiGe / Si (110), as a typical example of the STEM moiré. As a simple usage of this method, it is useful to distinguish coherent/incoherent interfaces. This method also has potential to analyze crystal-plane spacings and directions. One important point is that we don't need high-end TEM such as Cs-corrected machines.

## References:

[1] S. Kim et al., Appl. Phys. Lett. 102 (2013) 161604.

[2] Y. Kondo and N. Endo, Kenbikyo 49 (2014) 226, in Japanese.

[3] A. Ishizuka et al., J. Electron Microsc. 66 (2017) 217.

[4] A. Pofelski et al., Ultramicroscopy 223 (2021) 113225

[5] Junji Yamanaka et al., J. Mat. Sci. & Chem. Eng., 5 (2017) 102.

[6] Junji Yamanaka et al., Microsc. Microanal. 25 (Suppl 2) (2019) 242.

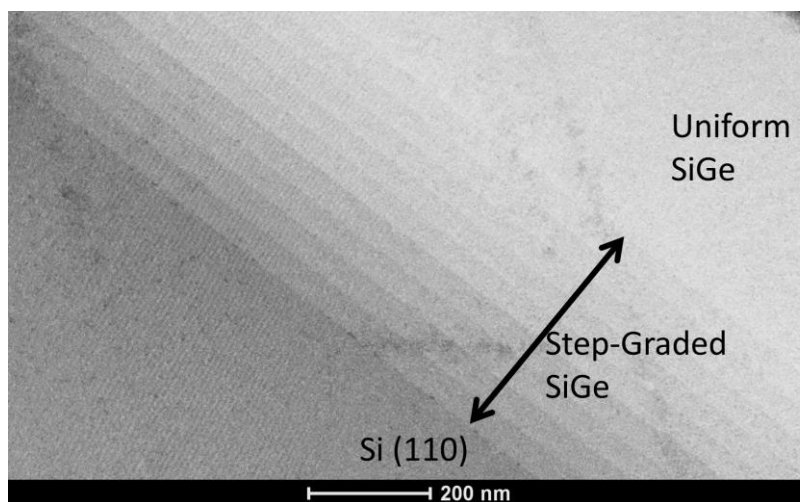


Fig. 1 STEM bright field image of the SiGe / Si (110). STEM moiré pattern is observed. A slight change of the moiré direction among different layers can be seen. This includes the information of the slight change of the crystal-plane spacing.

## **Development of Electron Microscopy toward Analysis of Optical and Quantum Effects in Nanomaterials.**

A. Maigné<sup>1\*</sup>, S. Patankar<sup>1</sup>, G. Sawatzky<sup>1,2</sup>, A. Nojeh<sup>1,3</sup>

<sup>1</sup> Stewart Blusson Quantum Matter Institutem, University of British Columbia, Vancouver, Canada.

<sup>2</sup> Department of Physics and Astrophysics, University of British Columbia, Vancouver, Canada

<sup>3</sup> Department of Electrical and Computer Engineering, University of British Columbia, Vancouver, Canada

\* alan.maigne@ubc.ca

In low-dimensionality objects such as nanowires and nanoparticles, material properties are drastically influenced by confinement effects. New physics rules the electronic and optical properties, which make designing and understanding nanomaterials so complex yet so appealing. For example, nanotube forests exhibit unique thermionic properties, and nanoparticles' optical response changes drastically with their size and surface chemistry. Understanding and tuning those effects is the key to designing nanoparticles and nanowires for applications such as quantum computing, solar cells and water treatment. Because characterizing such phenomena requires a combination of energy, momentum and spatial resolution, it remains extremely challenging.

During this presentation, we will discuss how to probe optical and quantum effects in a scanning transmission electron microscope through the use of momentum-resolved electron energy loss spectroscopy and cathodoluminescence.

## TEM at Millikelvin Temperatures: What Would It Be Useful for?

Hiroshi Okamoto<sup>1\*</sup>, Reza Firouzmandi<sup>2</sup>, Shota Uchita<sup>1</sup>, Vahid Sazgari<sup>2</sup> and Ismet I. Kaya<sup>2</sup>

<sup>1</sup> Department of Intelligent Mechatronics, Akita Prefectural University, 84-4, Aza Ebinokuchi, Tsuchiya, Yurihonjo, Akita 015-0055, Japan

<sup>2</sup> Faculty of Engineering and Natural Sciences, Sabancı University, Orhanli-Tuzla, Istanbul 34956, Turkey

\*okamoto@akita-pu.ac.jp

Much attention has been paid to experiments involving optical photons and free-space electrons recently [1]. Here we argue for potential interest and utility of *microwave photons* in this context and describe our effort being undertaken. As a result of extensive research in superconducting quantum computing [2], exquisite control over microwave photons is possible today [3]. Moreover, interaction between microwave photons and electrons could enable a rather unexpected application, namely high-resolution biological electron cryomicroscopy [4].

The central aspect of superconducting qubits that interests us is their ability to generate *quantum-mechanically superposed* electromagnetic fields around them. This would result in an interesting and exploitable interaction with flying electrons. For instance, a flux-qubit, in which an electric current as large as 1  $\mu\text{A}$  could flow in *both* clockwise and counterclockwise manner at the same time, produces a superposed magnetic field around it. Another possibility, unique in microwave frequencies, is to generate a superposed state of two very distinct electromagnetic fields involving  $\approx 100$  photons using the so-called bosonic qubit [3]. The latter possibility may be more practical for reasons to be detailed in the talk.

"Seeing" such a superposed electromagnetic field with a TEM would certainly constitute an intriguing physics experiment on its own. The price to pay is the necessity of millikelvin temperatures to ensure  $\hbar\omega > k_B T$ , where  $\omega \approx 10$  GHz is the microwave photon frequency. For this purpose, a <sup>3</sup>He/<sup>4</sup>He dilution refrigerator must be inserted in the TEM. Nonetheless, such effort may be amply rewarded because we do know a way to exploit electron-qubit interaction to eventually enable "quantum electron microscopy" of beam-sensitive biological specimens [4].

A project involving a TEM combined with a dilution refrigerator would be costly. For proof-of-principle purposes, instead we plan to place an "ultrasmall TEM" in a commercial dilution refrigerator. Development of such a small TEM, their test equipment, as well as superconducting devices, is underway (Fig. 1).

We thank Y. Okuda, Y. Takayama and S. Miura for their early contributions to the development of our experimental setups. This research is supported in part by the JSPS "Kakenhi" grant (Grant No. 19K05285).

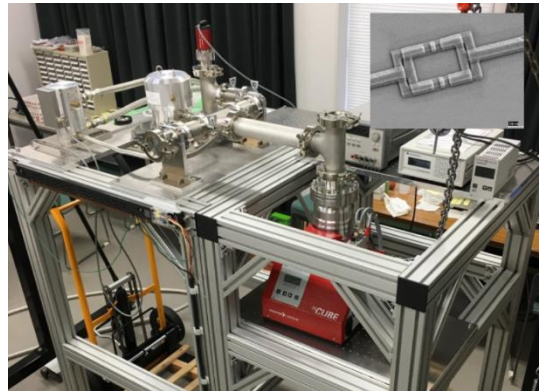


Fig. 1. Low temperature test equipment under construction. Inset: A Josephson device.

### References:

- [1] See e.g. K. Wang et al., *Nature* **582** (2020), 50–54; O. Schwartz et al., *Nat. Methods* **16** (2019) 1016-1020.
- [2] For a recent review, see e.g. P. Krantz et al., *Appl. Phys. Rev.* **6** (2019) 021318.
- [3] See e.g. B. Vlastakis et al., *Science* **342** (2013) 607-610.
- [4] H. Okamoto, *PRA* **85** (2012) 043810; H. Okamoto and Y. Nagatani, *APL* **104** (2014) 062604; H. Okamoto arXiv:2001.05603v3 [quant-ph].

## Higher-order structure of barley chromosomes observed by Electron Tomography.

Misa Hayashida<sup>1\*</sup>, Channarong Sartsanga<sup>2</sup>, Rinyaporn Phengchat<sup>2</sup>, Marek Malac<sup>1,2</sup>, Kiichi Fukui<sup>4</sup>, Nobuko Ohmido<sup>2</sup>

<sup>1</sup> Nanotechnology Research Centre, National Research Council, 11421 Saskatchewan Drive, T6G 2M9, Edmonton, Alberta, Canada.

<sup>2</sup> Graduate School of Human Development and Environment, Kobe University, 3-11 Tsurukabuto, Nada-ku, 657-8501, Kobe, Japan.

<sup>3</sup> Department of Physics, University of Alberta, Edmonton, Alberta T6G 2E1, Canada.

<sup>4</sup> Graduate School of Pharmaceutical Sciences, Osaka University, 1-6 Yamadaoka, Suita, Osaka 565-0871, Japan

\*misa.hayashida@nrc-cnrc.gc.ca

The higher order metaphase chromosome structure has been an enigma for over a century and several different models have been presented based on results by various imaging techniques. Some of the disagreements between methods have come from artifacts caused during sample preparation such as staining and dehydration.

Therefore, we treated unstained barley chromosomes with ionic liquid to prevent dehydration. Moreover, we observed chromosomes on a film with holes to prevent chromosomes from being flattened when placed on the film, as show in Fig. 1. A chromosome which made a bridge over a hole (Fig. 2) was mounted on a tomography holder [1], and observed its 3D structure using electron tomography. We found that there are periodic structures with 300-400 nm pitch along chromosome axis in barley chromosomes. The pitch size is larger than the pitch observed in human chromosomes [2].

### References:

[1] R. Phengchat et. al., *Micron*, 126, 102736 (2019)

[2] M. Hayashida et. al, *Microscopy and Microanalysis* (2021), 27, 149–155

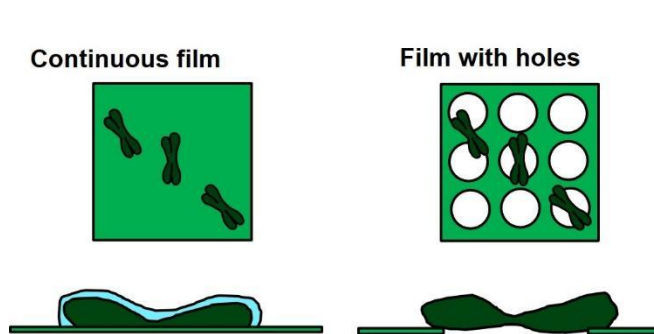


Fig. 1 Illustrations of a chromosomes on a continuous film and on a film with holes. The chromosomes were flattened on the film and sometimes excessive ionic liquid remained in the surface of the chromosomes when placed on a continuous film.

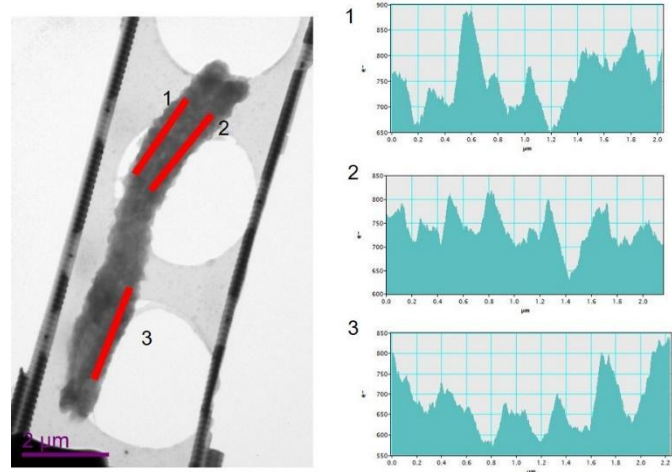


Fig. 2. A TEM image of an unstained barley chromosome and the line profiles, as indicated in red in the left image. A chromosome which made a bridge over a hole was observed.

## In-situ STEM observation of Ni catalyst during dry methane reforming

山本 知一(Tomokazu Yamamoto)<sup>1\*</sup>, 新村 光生(Mitsuki Shinmura)<sup>2</sup>, 松田 潤子(Junko Matsuda)<sup>3</sup>, 瓜田 幸幾(Koki Urita)<sup>4</sup>, 中越 修(Osamu Nakagoe)<sup>4</sup>, 松村 晶(Syo Matsumura)<sup>1, 2</sup>

<sup>1</sup> Ultramicroscopy Research Center, Kyushu University, 744 Motoooka, Nishi-ku, Fukuoka 819-0395, Japan.

<sup>2</sup> Department of Applied Quantum Physics and Nuclear Engineering, Kyushu University, 744 Motoooka, Nishi-ku, Fukuoka 819-0395, Japan.

<sup>3</sup> International Research Center for Hydrogen Energy, Kyushu University, 744 Motoooka, Nishi-ku, Fukuoka 819-0395, Japan.

<sup>4</sup> Graduate School of Engineering, Nagasaki University, 1-14 Bunkyo-machi, Nagasaki 852-8521, Japan

\*yamamoto@hvem.kyushu-u.ac.jp

Dry reforming of methane (DRM) with carbon dioxide (CO<sub>2</sub>) is has gained considerable research attention for a method to produce a syngas mixture of carbon monoxide (CO) and hydrogen (H<sub>2</sub>), which is a very important precursor for the production of a variety of valuable chemicals. Ni-based catalyst are known as active catalyst for dry reforming of methane. The degradation of catalytic activity due to the coking and sintering of catalysts remain a fundamental challenge. In this study, we investigated the graphite formation on Ni nanoparticles under DRM gas condition using in-situ STEM observation.

In-situ STEM observation of Ni/MgO-Al<sub>2</sub>O<sub>3</sub> catalyst was performed on a JEM-ARM200CF (JEOL) operated at 200 kV with a MEMS-type windowed gas-cell TEM holder system (Protochips Atmosphere 210). A mixed gas: CH<sub>4</sub>: 50 vol%, CO<sub>2</sub> vol%: 25, Ar: 25 vol% was flowed with 0.2 ml/min at a gas pressure of 101 kPa. The flowed gas was also analyzed by QMS. Temperature was ramped from 300 °C to 900 °C.

Fig.1 shows BF-STEM images of Ni nanoparticles under DRM condition. Graphite layer formation was observed around 800 °C. At this temperature, progress of DRM reaction was confirmed by gas analysis (Fig. 2). Nanoparticle surfaces were changed to be flat during graphite layer formation.

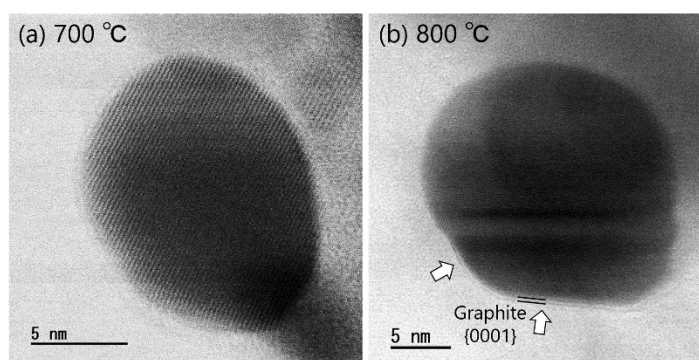


Fig. 1. BF-STEM images of Ni nanoparticles under a mixed gas (CH<sub>4</sub>: 50 vol%, CO<sub>2</sub> vol%: 25, Ar: 25 vol%) flow (a) at 700 °C and (b) at 800 °C.

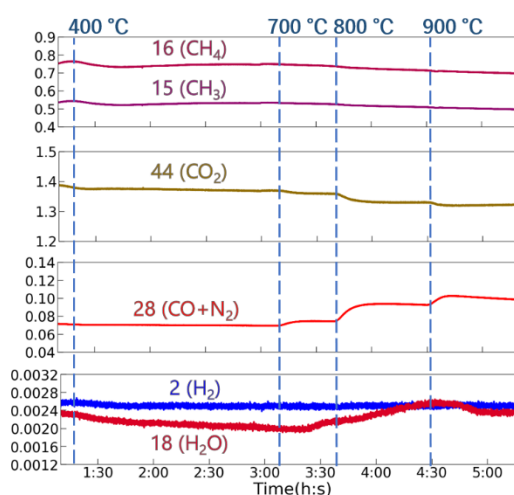


Fig. 2. The QMS data vs time. The MS intensity for each m/z channel was normalized by the intensity of Ar balance gas.

# STEM and EELS of Spontaneous Incommensurate van der Waals Heteroepitaxy

Hesham El-Sherif<sup>1,2</sup>, Stephen M. Jovanovic<sup>3</sup>, John Preston<sup>3</sup>, Nabil Bassim<sup>1,\*</sup>

<sup>1</sup> Materials Science and Engineering, McMaster University, Hamilton, Ontario, L8S 4L8, Canada

<sup>2</sup> (current address) Rowland Institute, Harvard University, Cambridge, Massachusetts, 02138, USA.

<sup>3</sup> Engineering Physics, McMaster University, Hamilton, Ontario, L8S 4L8 Canada.

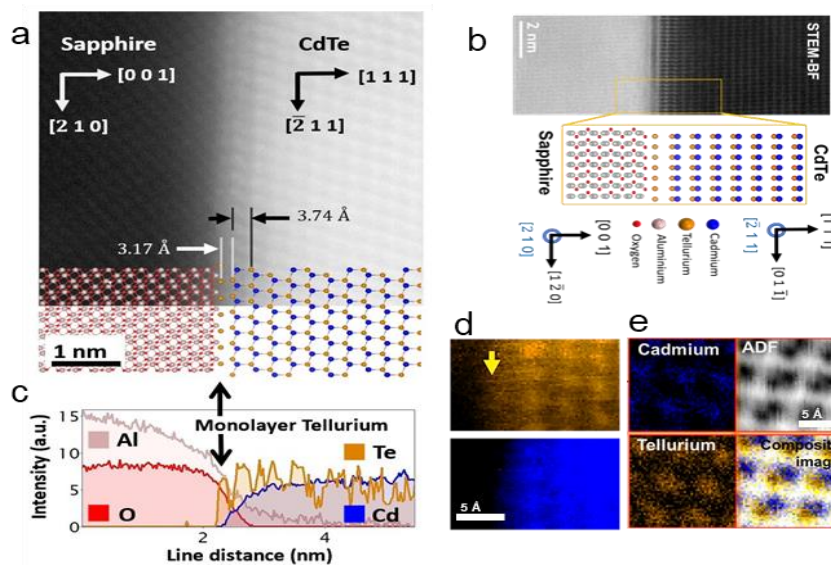
\*bassimn@mcmaster.ca

Heterogeneous integration of High-quality single-crystalline thin films may be achieved by in-situ fabrication or lift-off technologies from compliant substrates with remote and van der Waals epitaxy growth of semiconductors.[1] However, the quality of transferred semiconductor films depends on the quality and real-size of manually transferred two-dimensional (2D) materials, limiting the size of direct large-area single-crystal films.

In this presentation, a one-step growth method will be introduced to fabricate thin films that are incommensurate to their substrate through a spontaneous van der Waals-like epitaxy.[2] In this relatively low-temperature growth, a buffer layer of chalcogenide is spontaneously attached to the interface with a weak chemical interaction between a surface-reconstructed substrate and a 3D film. An epitaxial relationship between the substrate and film is maintained across this interfacial layer. Moreover, no mismatch dislocations are observed at the interface, which allows high-quality single-crystal thin film growth. This unique interface complexion allows for lift-off of films without first transferring a 2D material onto their growth substrate for remoting epitaxy.

The presentation will focus on the fundamental interface understanding of cadmium telluride (CdTe) on sapphire system, fabricated via pulsed laser deposition at 300 °C.[2, 3] In Fig. 1, a mono-layer of chalcogenide (tellurium) at the interface is examined by various spectroscopic scanning transmission electron microscopy (STEM) techniques, including low-loss and core loss electron energy-loss spectroscopy (EELS) to reveal both the bonding and chemical composition at the interface.

Fig. 1. Understanding the interface structure by Core-loss EELS and STEM imaging. (a and b) STEM-HAADF and STEM-BF images at the interface showing CdTe in the (011), and (11) directions, respectively. a monolayer tellurium is resolved in an EELS line scan in (c) and EELS area map in (d). The polarity of the film is Cd-polar as resolved by atomistic EELS mapping in (e).



## References

[1] S-H Bae et al., Nature Nanotechnology 15 (2020), p. 272.

[2] SM Jovanovic et al., Small 16 (2020), p. e2004437.

[3] H El-Sherif et al., Microscopy and Microanalysis 26 (2020), S2, p. 3116



JSM MSC PHOTOS-November 15, 2021

